State-Specific Spectral Doublets in the FTIR Spectrum of Gaseous Tropolone†

Richard L. Redington*

Department of Chemistry and Biochemistry, Texas Tech University, Lubbock, Texas 79409

Robert L. Sams

Environmental Molecular Sciences Laboratory, Pacific Northwest National Laboratory, Richland, Washington 99352

Received: June 13, 2001; In Final Form: September 17, 2001

The infrared absorption spectrum of tropolone vapor at 25 °C, ∼0.01 Torr, and 32 m path length has been recorded from 960 to about 700 cm^{-1} at a resolution of 0.0025 cm^{-1}. Twenty-nine cold band and hot band spectral tunneling doublets marked by sharp type A or type C Q branch apexes protruding from the congested vibration−contortion−rotation absorption profiles are assigned. Twenty-six vibration-contortion state-specific splittings are estimated for tropolone in its ground electronic state. This number is currently unprecedented in the literature for any sizable molecule. About half of these quasiharmonic vibrational states show an appreciable quenching of tunneling due to increased effective barriers and/or path lengths and, in the case of the nominal COH torsion, the tunneling is reduced to 0.07 of the zero-point (ZP) value of 0.974 cm^{-1}. The analysis is guided by predictions of the independent {tunneling skeleton}{tunneling H atom} tautomerization model that was previously applied to the vibrational spectrum and tautomerization mechanism of tropolone. The increase of effective tunneling path length by a few percent over the ZP path length is attributed to dynamical complexity arising from an atom-to-atom exchange of unequal vibrational displacements as a part of the tautomerization process. This aspect of tunneling quenching behavior can arise for quasiharmonic vibrations lacking direct contact to the OH···O group. For the case of tropolone, the tautomerization model advocates heavy atom tunneling as equal in importance to H atom tunneling. Heavy atom tunneling is supported by the observation of a (perturbed) spectral tunneling doublet at 754 cm^{-1} with the separation 0.80 cm^{-1}. This doubling of the high frequency component of the previously observed 11 cm^{-1} doublet observed using Ne matrix-isolation sampling provides evidence for the "doublet of doublet" quartet structure predicted for the ν_{37} nascent skeletal tunneling (contortion) vibration. The compilation of numerous vibrational state-specific tunneling doublings for a 15-atom nonrigid molecule invites further experimental and theoretical research aimed at advancing the understanding of multidimensional intramolecular tunneling dyanmics, vibrational energy redistribution, and unimolecular reaction kinetics. Several strong parallels are seen between the vibrational interactions arising in our studies of the tautomerization of tropolone and those appearing in recent articles discussing possible behaviors in the active sites of enzymatic H tranfer reactions.

1. Introduction

In 1972, Alves and Hollas[1,2] reported vibrational state-specific spectral tunneling doublets in the $S_1 \leftarrow S_0$ UV absorption spectrum of warm tropolone vapor, and in subsequent years laser excitation and dispersed fluorescence spectra of jet-cooled samples[3−9] revealed about a dozen vibrational state-specific tunneling doublets for the $S_1 \leftrightarrow S_0$ vibronic transitions of tropolone-oh (Tp-oh) and tropolone-od in the simplified cold spectra. In the S_1 ($\pi^*\pi$) electronic state the doubling separations range from unresolved values near zero to values reaching about 30 cm^{-1}. The studies of jet-cooled samples were extended to ^{18}O-labeled tropolones[10,11] and to ring-labeled tropolone derivatives[12−15] with the objective of understanding how couplings between the OH···O motion and other vibrations enter the intramolecular tunneling dynamics of a 15-plus atom nonrigid molecule. The observed vibrational state-specific tunneling behavior stimulated several theoretical/computational models.[16−23] These works have had to face the fact that the vibronic spectroscopy primarily characterized properties of the S_1 state, whereas quantum mechanical estimations of the potential energy surface (PES) supporting the dynamical behavior are very approximate. In general, the theoretical models have focused strongly on H atom behavior with little emphasis on detailed exposition of the heavy atom dynamics.

Our recent studies of Tp-oh and Tp-od[24,25] focused on the infrared vibrational spectra and tautomerization in the theoretically accessible S_0 electronic ground state. The IR spectral doublets are generally smaller than those in the vibronic spectra, but they are more numerous and probe a wide range of tunneling splitting behaviors. Low resolution IR absorption spectra of gaseous tropolone were reported by Ikegami[26,27] in the early 1960s, and improved IR absorption spectra for gaseous Tp-oh and Tp-od were published by Redington, Redington, and Montgomery.[24] Detailed vibrational assignments for the isotopomers were based on IR spectra measured in the vapor phase, isolated in Ne and Ar matrixes, and dissolved in CCl_4 and CS_2 solutions. In addition, the analysis utilized vibrational transitions reported for the 3100 cm^{-1} region of jet-cooled samples by

† Part of the special issue "G. Wilse Robinson Festschrift".

10.1021/jp0122631 CCC: $22.00
Published on Web 11/22/2001

Frost, Hagemeister, Arrington, and Zwier.[28] The analysis was made possible through high level MO quantum mechanical computations of the IR spectra and tautomerization mechanism.[24,25] In 1999, Tanaka, Honjo, Tanaka, Kohguchi, Ohshima, and Endo[29] published precise spectroscopic parameters for the zero-point (ZP) levels of S_0 tropolone including $\Delta_0 = 29\,193.788 \pm 0.026$ MHz for the ZP tunneling splitting (rounded to 0.974 cm^{-1} for use below).

The {tunneling skeleton}{tunneling H atom} tautomerization model[25] was developed through high level ab initio MO-computed points on the tropolone S_0 PES. The essence of this model derives from the OH stretching (ν_{27}) and skeletal contortional (ν_{37}) vibrational/tunneling computations on highly anharmonic one-dimensional (1-D) single- and double-well potential energy functions (PEFs) cut from the MO-based PES. The ν_{27} and ν_{37} vibrational cordinates are treated as adiabatically separated from each other; the 37 remaining fundamentals of tropolone are treated as harmonic oscillators. The OH stretching vibrational energies depend very strongly on the (frozen) contortion coordinate (i.e., on the heavy atom skeletal geometry). The dependence of the quasiharmonic vibrations on the skeletal geometry is much weaker. In each case, the dependence of the vibrational energies on the contorted skeletal geometry was estimated in the model,[25] with the results entered as dynamical energy contributions into the *effective* PEF governing the ν_{37} contortion vibration. The ν_{37} tunneling splittings were then computed for each of the vibrational state-spectfic ν_{37} 1-D effective PEFs.

The high quality MO computations show that the OH group remains localized until the 14-atom skeleton displaces to reach near-C_{2v} point group symmetry, and as this contortion proceeds the character of the OH···O PEF transforms from single-minimum to double-minimum to *equal* double-minimum. The latter character allows the H atom to delocalize between the O atoms and tautomerization to occur. The theoretical/computational tautomerization model has utilized no input of experimental information, whereas its predictions and guidance of the experimental analysis are strongly supported by the copious experimental data available for Tp-oh and Tp-od.

In the present paper, the MO-computed (harmonic) vibrational energies are introduced into the effective PEF previously obtained for the bare ν_{37} contortion coordinate[25] as a means to estimate the barrier perturbation caused by quasiharmonic excitations. The tunneling splittings computed for the ν_{37} ZP states using these new effective PEFs (for hot band transitions both the upper and lower generalized vibrational states are excited) then predict the spectroscopic tunneling doublet behavior as described below. The IR doublet separations are $\sim$1 cm^{-1} or less in the present spectrum and were not resolved in previous experimental studies. Only the highly anharmonic ν_{27} (OH stretching) and ν_{37} (contortion) vibrations, with fundamental doublet separations of 20 and 11 cm^{-1}, respectively,[24,25] were previously observed and assigned for Tp-oh and Tp-od in the IR. The ν_{37} transitions are at 754 and 743.4 cm^{-1} for neon-isolated Tp-oh, and each of these peaks should be additionally doubled by the zero-point splitting Δ_0 (vide infra). This doubling is reported here for the 754 cm^{-1} transition of Tp-oh vapor.

The results obtained for S_0 tropolone reflect on dynamical behaviors discussed, for example, by Kohen and Klinman,[30,31] Billeter, Webb, Iordanov, Agarwal, and Hammes-Schiffer,[32] and Antoniou and Schwartz[33] in context of the vibrational enhancement of H atom tunneling rates at the active sites of enzymatic H-transfer reactions. Some of the behaviors in common are (a) catalysis of H transfer via the transient equalization of PES minima resulting from appropriate skeletal (heavy atom) vibrational displacements; (b) the occurrence of nonadiabatic transitions (surface hopping) at avoided crossing points of the contortion-dependent OH stretching energy curves; (c) the necessity of utilizing higher dimensional vibrational subspaces for the coupled skeletal coordinates. The large amplitude H atom displacement and the shorter but significant heavy atom displacements that accompany the tautomerization of tropolone place strong emphasis on actual heavy atom tunneling phenomena. The behavior observed to occur in tropolones should plausibly lead to the recognition of similar behavior (when it arises under suitable conditions) in much larger (i.e., enzymatic/biological) systems. In prototypes provided by the tropolones, the occurrence of vibrational state-specific tunneling splittings opens direct windows on intramolecular dynamics that are only indirectly addressable through measurements of macroscopic kinetics and thermodynamics.

2. Experimental Procedures

Tropolone was purchased commercially, purified by sublimation, and placed in the sidearm of a folded-path IR absorption cell. Tropolone vapor diffused into the cell at its sublimation pressure of about 0.01 Torr at 25 °C, and the Bruker HR120 Fourier transform IR spectrophotometer was used to record absorption spectra of the gas at 32 m path length under spectral resolutions of 0.1 and 0.0025 cm^{-1}. The former involved 512 scans over about 40 min, the latter 128 scans over about 5 h of scan time. The high-resolution spectra were ratioed against background taken at 0.04 cm^{-1} resolution, with 128 scans and a times 16 zero fill to make the two spectra compatible. The smooth background introduced no noise into the ratioed spectra. The high-resolution spectra were calibrated against CO_2 at 667 cm^{-1} (HITRAN 96 version). The 0.0025 cm^{-1} resolution spectrum reveals intense pileups of Q branch transitions that are too narrow to be studied under 0.1 cm^{-1} resolution. Transitions due to traces of water, CO_2, CO, acetic acid, and possibly to other impurities in the system presented no recognized problems with respect to the spectral analysis presented for tropolone.

3. Overview of the IR Spectrum of Tropolone Vapor

As a rigid molecule tropolone would have C_s point group symmetry with 27 in-plane and 12 out-of-plane fundamental vibrations. At 750 cm^{-1} and 298 K the computed Doppler width of a vibration−rotation transition is 0.000 35 cm^{-1}. This line width is about one-seventh the 0.0025 cm^{-1} spectral resolution used in this work, and it precludes line analysis in the rotationally unresolved FTIR spectrum. Small rotational constants[29] ($A \approx 0.091$, $B \approx 0.055$, and $C \approx 0.034$ cm^{-1}) generate a dense manifold of rotational transitions for each vibration-contortion state. The spectral density of the observed absorption profiles at 25 °C is increased by the presence of hot bands and, often, by overlapping cold band(s).[24] The use of 0.0025 cm^{-1} resolution is nevertheless justified because of the sharp Q branch apexes that are observed for transitions with type A or type C rotational contours. Modeled as a rigid asymmetric top molecule with the asymmetry parameter $\kappa = -0.263$, the tropolone IR absorption profiles fall between those computed for model rotors #3 and #4 of Ueda and Shimanouchi.[34] The sharp type A and type C rigid rotor Q branch structures stand out prominently over modest P and R branch wings, whereas the type B contours totally lack sharp Q branch spikes. The estimated separation of the P and R branch maxima is $[(A + B + C)T]^{1/2} = 7.3$ cm^{-1}

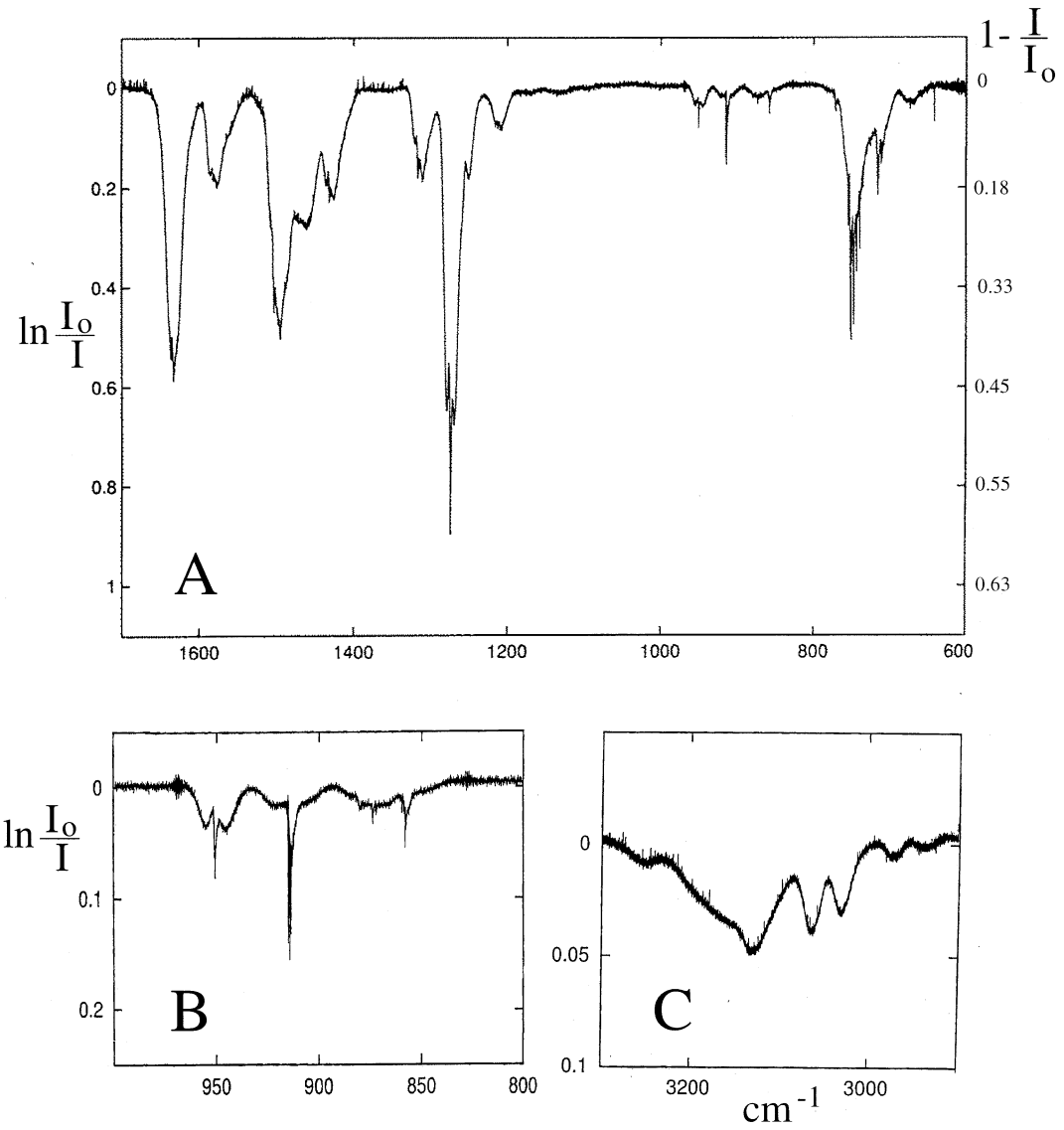

Figure 1. Overview of the FTIR absorption spectrum of gaseous tropolone at 25 °C, ~0.01 Torr, 32 m of path length and 0.1 cm^{-1} resolution. (A) 600−1700 cm^{-1} region. (B) Closeup showing type A (951 cm^{-1}) and type C (915 cm^{-1}) rotational profiles. (C) The fundamental OH/CH stretching region around 3100 cm^{-1}.

at 298 K.[34] An overview of the IR spectrum of tropolone vapor at 25 °C is shown in Figure 1A, with the 800−1000 cm^{-1} region shown in more detail in Figure 1B. The four fundamentals observed in this region are each closely overlapped by hot bands, but the observed 951 and 915 cm^{-1} profiles nevertheless strongly resemble the computed type A and type C contours,[34] respectively, of the rigid asymmetric rotor.

As a nonrigid tunneling molecule the molecular symmetry group[35] of tropolone is G_4, isomorphic to the C_{2v} point group, with group operations E, P, E^*, and P^*. The permutation P exchanges the O atoms, three pairs of C atoms, and two pairs of H atoms as shown for the tautomers in Figures 2A and 2B. The C_{2v} reference configuration, i.e., the saddle-point (SP) shown in Figure 2C, determines the irreducible representations for the fundamentals as $\Gamma_{vib} = 14A_1 + 13B_2 + 5A_2 + 7B_1$ (C_{2v} notation). The contortion (nascent skeletal tunneling) vibration ν_{37} and the OH stretching vibration ν_{27} are B_2. MO-computed normal coordinates for tropolone-oh have been presented at the RHF/6-31G level[36] and at the higher level conveniently designated MP2/GEN[24] [6-311G(df,pd) basis for atoms of the COH···OC chelate ring and 6-311G(d,p) for atoms of the C_5H_5 loop]. The Gaussian 98 codes were used in this work.[37] MP2/GEN computed normal modes for tautomer vibrations of interest to the present work are shown in Figures 3 and 4 and, because it is needed below, the MP2/GEN computed harmonic frequency of the C_{2v} SP configuration is listed in the first line below each Q_V.

The spectral doublet separations are related to the upper state Δ' and lower state Δ'' tunneling splittings as $|\Delta' \pm \Delta''|$. The selection rules are illustrated in Figure 5 for the four types of cold band transitions and, on the right, for one example of a hot band (a $\nu + \nu_{19} - \nu_{19}$ transition for a vibration ν with B_1 symmetry). Figure 2A,[38] and Figures 3 and 4, suggest many in-plane vibrational motions can generate simultaneous transition dipole components along the two in-plane principal axes. In the present FTIR data only the Q branches of type A contours are observed (because of their sharpness) since the Q branch rotational transitions of type B contours are relatively dispersed and hence not identifiable in the dense general absorption. Q branches of the type C contours (out-of-plane vibrations) are sharp and, like the type A Q branches, identifiable in the spectrum.

The IR spectra of tropolones, particularly the peak intensities, depend on sampling conditions[24] including the temperature. A

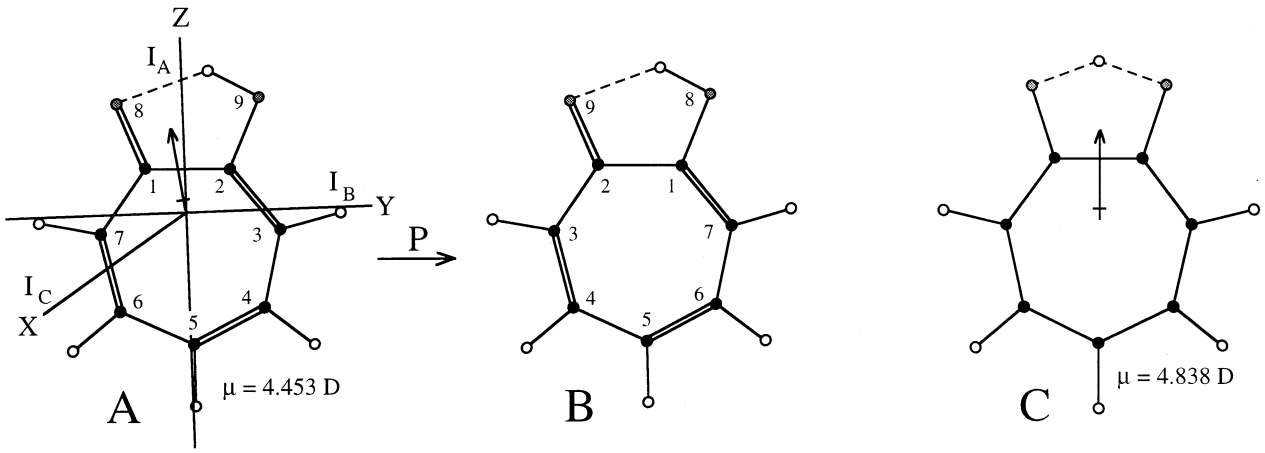

Figure 2. (A) Inertial principal axes of tropolone. (B) Tautomer obtained via the permutation P of the C, CH, and O entities. (C) C_{2V} saddle-point configuration. The permanent dipole moments are MP2/GEN computed.

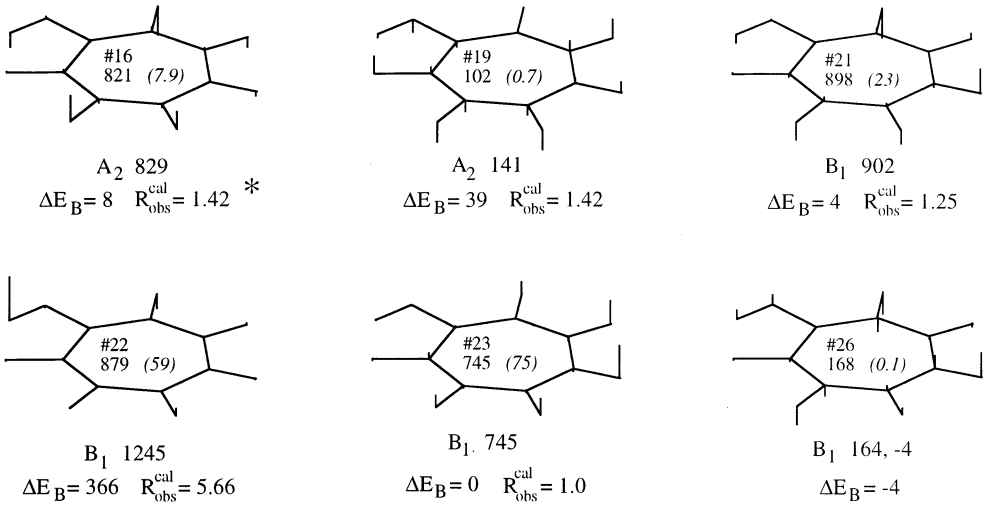

Figure 3. MP2/GEN computed out-of-plane normal coordinates for the tautomer. The mode number, harmonic frequency (cm^{-1}) and IR absorbance (km) are reported within each ring. Irreducible representations in the G_4 molecular symmetry group and the MP2/GEN-computed harmonic vibrational frequency of the C_{2v} saddle-point configuration are listed in the first line below each ring. See text for ΔE_B and R_{obs}^{cal} definitions. The latter were calculated using paths p_1/p_1 and spectral doublets observed in this work.

comparison of the absorption contours recorded at 25 °C (Figure 1A) with data presented in ref 24 for 80 °C sampling shows very clearly the increased bandwidths attributable to increased hot band absorption at the higher temperature. In this paper absorbance, $\ln(I_o/I)$, is used as the spectral intensity coordinate. Absorbance enhances the strength of intense peaks relative to the weak and, for reference, coefficient of absorption values ($1 - I/I_o$) are included as the right side ordinate of Figure 1A.

In addition to providing pronounced hot band activity[39] the lowest frequency fundamentals (110 and 177 cm^{-1}) are notable because many of their overtone and combination states appear in the $S_1 \leftrightarrow S_0$ vibronic spectrum of warm bulb[40] gaseous tropolone samples. More generally, comparisons between IR spectra obtained for warm gaseous and cold matrix-isolated tropolone reveal that there is an exceptionally large number of overtone and combination transitions in the spectra.[24] The intensities of these transitions are generally highly sensitive to the anharmonic couplings. The latter frequently link several fundamental, overtone, and combination states into resonance networks.[24] Absorbance behavior in the OH/CH stretching region around 3100 cm^{-1} is illustrative: the composite cold band plus hot band absorption profiles obtained at 25 °C and 80 °C[24] both extend between the limits of 2900 and 3300 cm^{-1} covered in Figure 1C, whereas cold band profiles of jet-cooled[28] and Ne matrix-isolated[24] samples span the 2975 to 3175 cm^{-1} range. Thus, about half of the 400 cm^{-1} range covered by the vapor phase absorptions is attributable to hot band transitions. The broad cold band absorption is understandable in terms of the OH/CH fundamentals resonantly coupled to numerous intense binary overtone and combination transitions.[24] The 3100 cm^{-1} region has, as yet, revealed no evidence for sharp Q branch peaks.

The evaluation of most upper state vibration-contortion-rotation parameters for S_0 tropolone must await the application of ultrahigh-resolution laser spectroscopy to temperature-dependent bulb samples and to jet-cooled samples. At present, about a dozen spectroscopic parameters for the zero-point levels of S_0 tropolone are known through the microwave study by Tanaka et al.,[29] of which their value for Δ_0 is critical to the following analysis.

4. Preliminaries to Spectral Tunneling Analysis

Vibrational states which enhance tunneling relative to the zero-point value may act by (a) lowering the effective PES barrier, (b) equalizing energies of the PES minima, or (c) shortening the tunneling pathway, while states which quench tunneling behave oppositely. Systematic analysis of the many

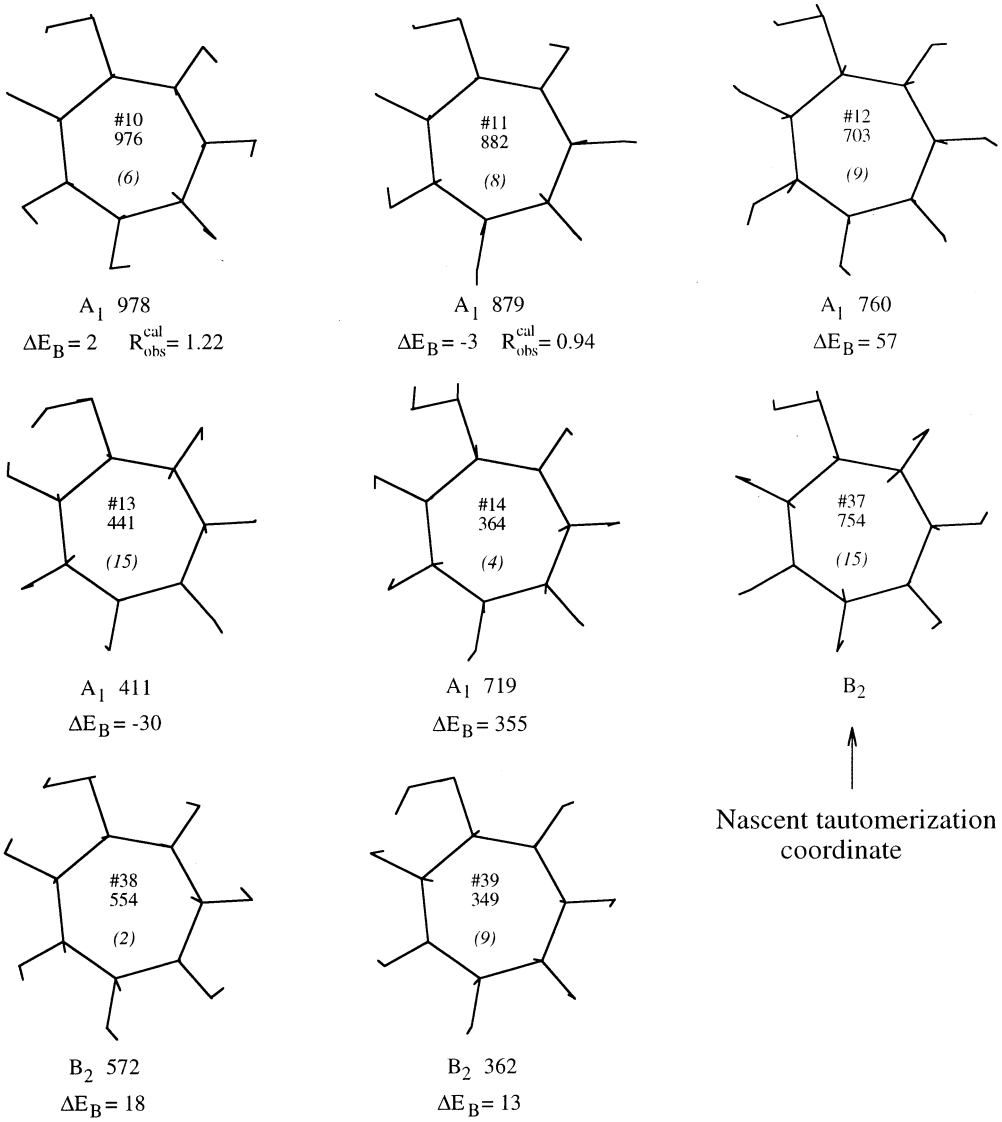

Figure 4. MP2/GEN computed in-plane normal coordinates for the tautomer; cf. Figure 3.

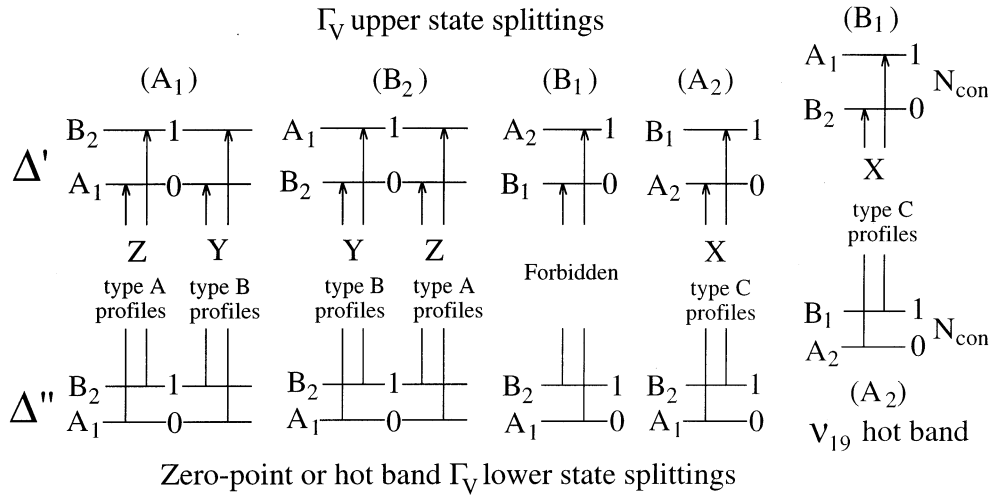

Figure 5. Vibration-contortion transitions between quasiharmonic states of tropolone. N_{con} is the contortional quantum number,[35] i.e., the quantum number labeling individual tunneling states of ν_{37} (cf. Figure 6).

IR tunneling doublets presented below utilizes the guidance, notation, and semiquantitative state-specific tunneling doublet predictions of the {tunneling skeleton} {tunneling H atom} model.[25] It is used to assess point (a) above, whereas the PES symmetry obviates point (b). The impact of point (c) is judged through comparisons between the calculated and observed vibrational state-specific tunneling separations.

Vibrational State-Specific Tunneling Barriers; [Point (a)]. Figure 6A shows double-minimum quadratic-quartic-Gaussian functions representing effective 1-D PEFs for the ν_{37} contortion

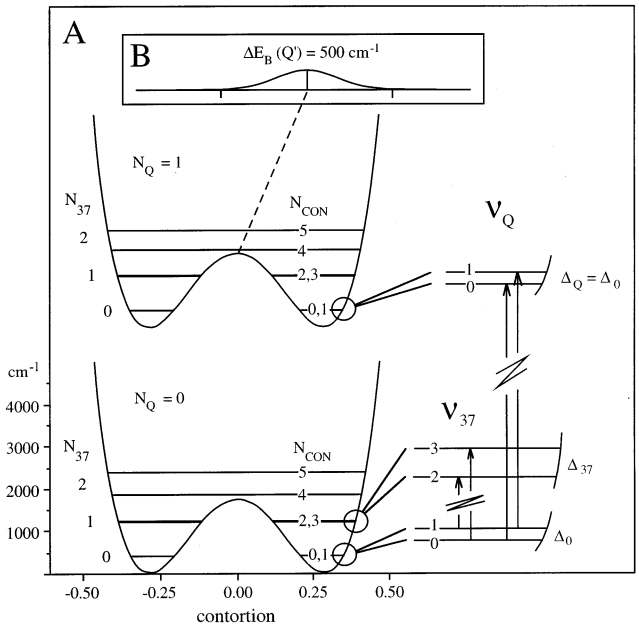

Figure 6. (A) One-dimensional effective PEFs for the nascent tautomerization (contortion) vibration ν_{37} of tropolone-oh. The curves are quadratic−quartic-Gaussian functions parametrized by purely quantum mechanical input.[25] The lower curve determines ν_{37} vibrational/tunneling states when all other vibrations are in their zero-point levels. The upper curve determines the ν_{37} energy states when one quasiharmonic fundamental, ν_Q, is excited. It is identical to the lower state because the vibration ν_Q is assumed to show no interaction with the contortion coordinate. The ν_Q transitions are drawn assuming ν_Q is of species A_1 with a Z polarized transition dipole. The ν_{37} transitions are for the Z polarized transition dipole. (B) Gaussian function representing the vibrational energy contribution to the effective PEF for ν_{37} from a path-active vibration $\nu_{Q'}$. The Gaussian would be added to the upper curve to describe the effective PEF for ν_{37} when the $\nu_{Q'}$ fundamental is excited. State $\nu_{Q'}$ adds 500 cm^{-1} to the effective barrier maximum. See text.

(nascent skeletal tunneling) vibration. In the lower (ZP) curve no vibrations are excited while in the upper curve a single totally tautomerization path-passive quasiharmonic fundamental ν_Q is excited. The quadratic−quartic component of the ν_{37} effective PEF for the ZP is parametrized by MO-computed energies (MP4/GEN//MP2/GEN) obtained at the optimized tautomer and C_{2v} saddlepoint geometries. The Gaussian component represents the difference between the summed ZP vibrational energies of the tautomer and those of the C_{2v} SP (of course, ν_{37} is not included). The dependence of this vibrational energy on the contortion coordinate is given Gaussian functionality in lieu of detailed knowledge of the molecular PES. The Gaussian approximation is convenient for the computation of PEF matrix elements entering the ν_{37} vibrational secular equation. Except for the ν_{27} (OH stretch) contribution, the Gaussian function is parametrized using MO-computed harmonic fundamental frequencies (MP2/GEN). The 1-D OH···O PEF is fitted to MP4/GEN computed points of the molecular PES, and the highly anharmonic ν_{27} energies are computed via a secular equation.[25]

In the upper curve, the ν_Q fundamental is excited but it does not affect the tunneling because the ν_Q vibrational coordinate is (in the example) independent of the contortion. The fundamental frequency is then nearly the same at the tautomer and C_{2v} SP geometries and the Gaussian contribution from this excited state is nil. The transitions illustrated for ν_Q assume it has A_1 symmetry and a Z-polarized transition dipole (cf. Figure 5). The tunneling doublet separation $|\Delta' - \Delta''|$ is zero.

Unlike the example for ν_Q the vibrational energies for a tautomerization path-active vibration $\nu_{Q'}$ differ at the C_{2v} SP and tautomer configurations. Thus, an additional Gaussian contribution must be added to the ν_{37} ZP effective PEF. The maximum of this Gaussian is $\Delta E_B(Q') = [\omega_{Q'}(C_{2v}\ SP) - \omega_{Q'}(taut)]$. At the tautomer configuration the value of the Gaussian is reduced to $0.02\Delta E_B(Q')$, with the factor 0.02 arbitrarily chosen to scale the breadths of all Gaussians.[25] In Figure 6B, it is assumed for illustration that $\Delta E_B(Q') = 500\ cm^{-1}$. Adding this function to the upper double-minimum curve raises the barrier of the resulting effective PEF, but not its qualitative shape. The shape of the effective PEF for ν_{37} is strongly altered upon excitation of ν_{27} (OH stretch).[25]

TABLE 1: In-plane Fundamentals and $\Delta E_B(N)$ Barrier Height Adjustments for tropolone-oh

A_1 vibrations				B_2 vibrations			
N	alt.[a]	ν_{obs}[b]	$\Delta E_B(N)$[c]	N	alt.	ν_{obs}	$\Delta E_B(N)$
1	(2)	3071	0	27	(1)	3121, 3102	[NA][d]
2	(4)	3071	4	28	(3)	3071	4
3	(6)	3034	1	29	(5)	3034	−2
4	(7)	1632	444	30	(8)	1616.0	127
5	(9)	1581.1	73	31	(10)	1565.0	47
6	(11)	1498.8	61	32	(13)	1413.6	67
7	(12)	1431	−15	33	(14)	1315	55
8	(15)	1273.5	63	34	(16)	1253.3	17
9	(18)	1207.5	3	35	(17)	1214.2	21
10	(20)	950.7	2	36	(19)	(1051)	22
11	(21)	874	−3	37	(22)	754, 743.4	[18][d]
12	(23)	675	51	38	(24)	552	18
13	(25)	436	−30	39	(27)	349.1	13
14	(26)	361.1	355				

[a] Alternative numbering used in ref 24 (nontunneling molecule with C_s point group). [b] Observed fundamentals taken from ref 24. [c] MP2/GEN computed $\Delta E_B(N) = \omega_N(C_{2v}$ saddle-point$) - \omega_N$(tautomer). The ω_N(tautomer) fundamentals are listed in ref 24. [d] Quasiharmonic $\Delta E_B(N)$ values are not applicable to the highly anharmonic coordinate subspaces of ν_{27} (OH stretch) and ν_{37} (contortion).

TABLE 2: Out-of-plane Fundamentals and $\Delta E_B(N)$ Barrier Height Adjustments for tropolone-oh

A_2 vibrations				B_1 vibrations			
N	alt.[a]	ν_{obs}[b]	$\Delta E_B(N)$[c]	N	alt.	ν_{obs}	$\Delta E_B(N)$
15	(28)		−9	20	(29)		4
16	(32)	857.7	8	21	(30)	913.6	4
17	(34)		20	22	(31)	751.3	366[d]
18	(37)	271	23	23	(33)	714.5	0
19	(39)	110	39	24	(35)		5
				25	(36)		−5
				26	(38)	177	−4

[a−c] As in Table 1. [d] ν_{22} is the COH torsion vibration.

Tables 1 and 2 summarize properties of the tropolone fundamentals including ΔE_B values ranging from 444 cm^{-1} for ω_4 to −30 cm^{-1} for ω_{13}. The energy difference between the $[N_{37} = 0, N_{CON} = 0]$ and $[N_{37} = 0, N_{CON} = 1]$ states yields the state-specific tunneling splitting Δ_V for each fundamental ω_V. The procedure described for the estimation of $\Delta E_B(\omega_V)$ for a fundamental vibration is generalized to any overtone or combination vibrational state through the use of the summed harmonic fundamental energies.

Tunneling Path Lengths; [Point (c)]. The so-called "model" tautomerization pathway for tropolone was derived in ref 25, where it is called path D (aka path p_1 in the present work). The path is illustrated by the heavy line connecting tautomers T and T′ in Figure 7B, where it is represented by changes in the CO bond distances expressed as a function of the O···O distance. The ν_{37} skeletal contortion displacement follows the curved minimum energy path (MEP) before shortcutting it at an R(O···O) value leading past the SP of the *effective* energy ridge crest

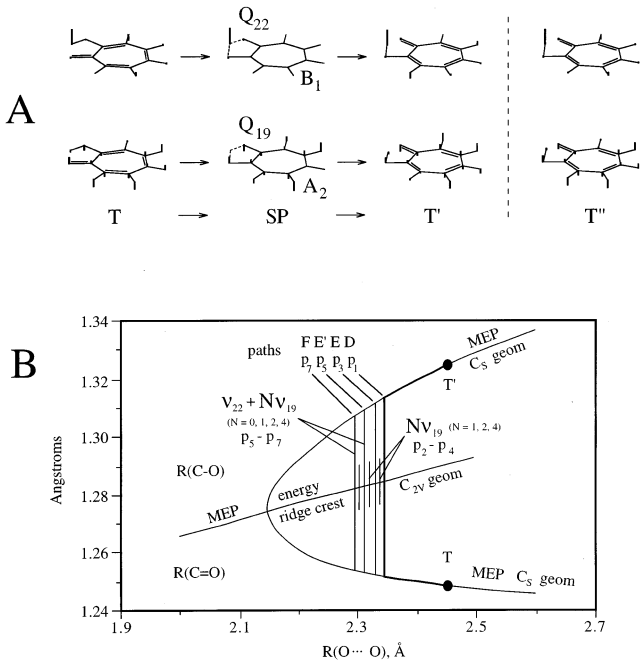

Figure 7. (A) Normal mode vibrational displacements accompanying the tautomerization of tropolone in the ν_{22} and the ν_{19} fundamental excited states. The comparison structure T″ has the geometry of T′ and the vibrational displacments of T. (B) The curved path represents the minimum energy path as expressed by CO bond distances calculated as a function of R(O···O).[25] The tautomerization path includes a shortcut at the saddlepoint along the energy ridge separating the two tautomer valleys. Path D (p_1) of the ZP and path-passive vibrational excited states is accented with a heavy line. The spread of elongated paths taken by the tautomerization path-active $N_{19}\nu_{19}$ fundamental and overtone states, and by the ν_{22} fundamental and $\nu_{22} + N_{19}\nu_{19}$ combination states are indicated. See text.

dividing the tautomer regions of the PES. On this ridge and at the SP the skeletal geometry [exclude H in OH···O] has C_{2v} point group symmetry. The tunneling splitting values computed for the excitation of ν_{37} are shown as Δ_0 and Δ_{37} in Figure 6A, along with transitions for the Y polarized transition dipole. Splittings computed for path D (p_1) are in good agreement[25] with the IR spectral data for neon-isolated Tp-oh and Tp-od. The Δ_0 value computed for Tp-od falls in the range prescribed by the available NMR data,[41] however, the $\Delta_0 = 0.2072$ cm^{-1} ZP tunneling splitting computed for Tp-oh using path D (p_1) is less than one-quarter of the 0.974 cm^{-1} observed[29] value. Because of this quantitative limitation the currently unrefined tautomerization model is used to compute theoretical splitting ratios $f_\tau^{\text{cal}}) = \Delta'/\Delta''$ of Δ' (upper state) and Δ'' (lower state) splittings for FTIR transitions cataloged by τ in Tables 3−5. The computed f_τ^{cal} ratios and corresponding experimentally determined ratios f_τ^{obs} are compared as $f_\tau^{\text{cal}}/f_\tau^{\text{obs}} = R_{\text{obs}}^{\text{cal}}$. Quasiharmonic vibrations that interact very little with the contortion coordinate are expected to yield $R_{\text{obs}}^{\text{cal}}$ values very near unity. Quasiharmonic vibrations which strongly quench tunneling will yield $R_{\text{obs}}^{\text{cal}}$ values that are much larger than unity. It is found that about one-half of the presently observed transitions are calculated (path p_1), and observed, to yield large values for $R_{\text{obs}}^{\text{cal}}$.

Quasiharmonic Vibrational Displacements and Tunneling Pathlenghs. Some tropolone fundamentals, e.g., ν_{23}, ν_{10}, and ν_{11}, are predicted to be tautomerization path-passive states. This is because MP2/GEN computed normal coordinates for the tautomer are virtually identical to the corresponding normal coordinates for the C_{2v} SP configuration, and yield near-zero

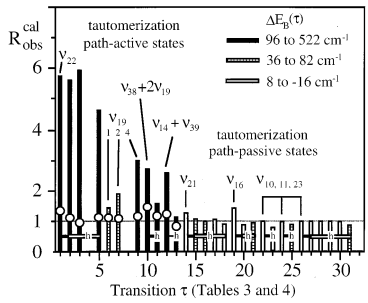

Figure 8. Bar graph comparing $R_{\text{obs}}^{\text{cal}}$ values for the assigned transitions. Model path D (p_1) is used for both the upper state and the lower state. Associated hot band transitions are grouped together and labeled by "h". White circles label near-unity $R_{\text{obs}}^{\text{cal}}$ values obtained using various elongated paths (cf. Figure 7B) for path-active vibrational states (cf. text and Tables 3 and 4).

ΔE_B(V) values as well. For path p_1 the $R_{\text{obs}}^{\text{cal}}$ ratios for ν_{23}, ν_{10}, and ν_{11} are expected and observed to be very near unity.

Other fundamentals, e.g., ν_{22}(COH torsion) and ν_{19}(OCCO/skeletal twisting), produce large ΔE_B(V) values. For the model (ZP) path p_1 they yield $R_{\text{obs}}^{\text{cal}} > 1$ because the f_τ^{cal} value is large. Decreased tunneling splittings yielding $R_{\text{obs}}^{\text{cal}}$ values near unity result upon increasing the effective tunneling path lengths of path-active vibrations by 5 or 10% over p_1.

Q_{23}, Q_{10}, and Q_{11}, with B_1, A_1, and A_1 irreducible representations in group G_4, respectively, change only slightly upon contortion. Their behavior is very different from that seen for the examples of Q_{22} (COH torsion) and Q_{19} (OCCO/skeletal twisting) shown in Figure 7A for the tautomer and C_{2v} SP configurations along the T → SP → T′ tautomerization. Both vibrations show that a specific atom-to-atom redistribution of the vibrational displacements must occur across the molecule for tautomerization to occur between energetically identical configurations T and T′. To provide a comparison, configuration T″ shows tautomer T′ carrying the same quasiharmonic vibrational displacements as tautomer T. Structure T″ is shown to (a) re-emphasize the particular atom pairs which exchange vibrational amplitudes during the tautomerization, and to (b) stress the high energy expected for the T″ configuration because of its large departure from normal coordinate displacements.

The optimal tautomerization pathway occurring in a quasiharmonic vibrational state that must redistribute its vibrational displacements is heuristically represented in this work by a slight increase in the effective tunneling path length over p_1 (the ZP value). Representative trial paths p_2 to p_7 are shown in Figure 7B. These longer path lengths are intended to reflect the intramolecular search for a minimum energy tunneling route between tautomers when the process includes added complexity for an atom-to-atom rearrangement of vibrational displacements across the molecule. Paths p_2 to p_7 in Figure 7B are taken as crossing the ridge crest in the effective PES at saddle-points shifted slightly from the p_1 SP because of the added multidimensional dynamical complexity. Parameters describing paths D, E, and F appear in Table 4 in ref 25 and those for intermediate paths in the p_1 to p_7 set were generated[42] to provide roughly equal path length increments.

Figure 8 summarizes the $R_{\text{obs}}^{\text{cal}}$ values obtained for the spectral transitions described in the following sections. The bars show $R_{\text{obs}}^{\text{cal}}$ values computed using equal upper and lower state model paths (p_1/p_1) to calculate $f_\tau^{\text{cal}} = \Delta'/\Delta''$. About half of the observed transitions yield $R_{\text{obs}}^{\text{cal}}$ ratios near unity to suggest lack of involvement of many vibrational states in the tautomerization

TABLE 3: Spectral Doublets and Tunneling Splittings (cm^{-1}) for Tautomerization-path-active Quasiharmonic Vibrations

	transition[a]			doublet origins		doublet separation		tunneling splittings[b]		$f = \Delta'/\Delta''$ paths Δ'/Δ''[c]			$f = \Delta'/\Delta''$ extended paths[d]			calc. barr. change[e]
τ	U	L	assignment	ν^{hi}	ν^{lo}	(±)	$\lvert\Delta' \pm \Delta''\rvert$	Δ'	Δ''	f_τ^{obs}	f_τ^{cal}	R_{obs}^{cal}	paths	f_τ^{cal}	R_{obs}^{cal}	$\Delta E_B(\tau)$
1	B_1	A_1	ν_{22}	752.02	751.12	(−)	0.90	0.074	[Δ_0]	0.076	0.43	5.7	p_5/p_1	0.101	1.33	366
2	B_2	A_2	$\nu_{22} + \nu_{19} - \nu_{19}$	747.97	747.41	(−)	0.56	[0.047]	0.61	0.077	0.43	5.6	p_6/p_2	0.084	1.09	405, 39
3	B_1	A_1	$\nu_{22} + 2\nu_{19} - 2\nu_{19}$	743.77	743.38	(−)	0.39	[0.031]	0.42	0.074	0.44	5.9	p_7/p_3	0.070	0.95	444, 78
4	B_2	A_2	$\nu_{22} + 3\nu_{19} - 3\nu_{19}$		739.28	(−)		[0.025]			0.44		p_7/p_4	0.104		483, 117
5	B_1	A_1	$\nu_{22} + 4\nu_{19} - 4\nu_{19}$	735.10	734.90	(−)	0.20	[0.021]	0.22	0.095	0.44	4.6	p_7/p_4	0.106	1.12	522, 156
6	A_2	A_1	ν_{19}					0.61	[Δ_0]	0.63	0.91	1.4	p_2/p_1	0.69	1.10	39
7	A_1	A_1	$2\nu_{19}$					0.42	[Δ_0]	0.43	0.83	1.9	p_3/p_1	0.47	1.08	78
8	A_2	A_1	$3\nu_{19}$						[Δ_0]		0.76		p_4/p_1	0.29		117
9	A_1	A_1	$4\nu_{19}$					0.22	[Δ_0]	0.23	0.69	3.0	p_4/p_1	0.26	1.13	156
10	B_2	A_1	$\nu_{38} + 2\nu_{19}$	773.07	771.80	(+)	1.27	0.30	[Δ_0]	0.30	0.80	2.7	p_3/p_1	0.45	1.45	96
11	B_1	A_2	$\nu_{38} + 3\nu_{19} - \nu_{19}$	772.51	771.59	(+)	0.92	0.31	[0.61]	0.51	0.80	1.6	p_3/p_2	0.59	1.16	135, 39
12	B_2	A_1	$\nu_{14} + \nu_{39}$	711.28	710.12	(+)	1.16	0.19	[Δ_0]	0.19	0.43	2.3	p_3/p_1	0.23	1.21	368
13	B_1	A_2	$\nu_{14} + \nu_{39} + \nu_{19} - \nu_{19}$	712.19	711.35	(+)	0.84	0.23	[0.61]	0.38	0.43	1.1	p_3/p_2	0.31	0.82	407, 39

[a] Irreducible representations (G_4) for the $N_{con} = 0$ level of the upper and lower vibrational states. τ is an identification number. [b] The fixed values for Δ are bracketed; see text. [c] Paths $\Delta'/\Delta'' = p_1/p_1$. For p_1 the computed Δ'' values in f_τ^{cal} are $\Delta_0 = 0.2072$, and $\Delta_{19}^N = 0.1887$, 0.1720, 0.1569, and 0.1432 cm^{-1} for $N = 1-4$; see text. [d] For paths $p'/p'' = p_m/p_n$ the Δ'' values in f_τ^{cal} are $\Delta'' = 0.2072$ for cold bands (i.e., ZP, p_1). For hot bands $\Delta'' = 0.1432$ (i.e. ν_{19}, p_2), 0.0965 ($2\nu_{19}$, p_3) 0.0596 ($3\nu_{19}$, p_4), and 0.0540 ($4\nu_{19}$, p_4). [e] MO computed $\Delta E_B(\tau)$ values are listed for the upper state, and for lower states with nonzero values (i.e., $N_{19}\nu_{19}$ hot bands).

TABLE 4: Spectral Doublets and Tunneling Splittings (cm^{-1}) for Tautomerization-path-passive Quasiharmonic Vibrations

	transition[a]			doublet origins		doublet separation		tunneling splittings[b]		$f = \Delta'/\Delta''$ paths Δ'/Δ''[c]			$f = \Delta'/\Delta''$ extended paths[d]			calc. barr. change[e]
τ	U	L	assignment	ν^{hi}	ν^{lo}	(±)	$\lvert\Delta' \pm \Delta''\rvert$	Δ'	Δ''	f_τ^{obs}	f_τ^{cal}	R_{obs}^{cal}	paths	f_τ^{cal}	R_{obs}^{cal}	$\Delta E_B(\tau)$
14	B_1	A_1	ν_{21}	915.142	914.942	(−)	0.200	0.77	[Δ_0]	0.79	0.99	1.25	p_2/p_1	0.75	0.95	4
15	B_2	A_2	$\nu_{21} + \nu_{19} - \nu_{19}$	914.369	914.327	(−)	0.042	0.57	[0.61]	0.93	0.99	1.06	p_2/p_2	0.99	1.06	43, 39
16	B_1	A_1	$\nu_{21} + 2\nu_{19} - 2\nu_{19}$	913.827	913.785	(−)	0.042	0.38	[0.42]	0.90	0.90	1.00	p_3/p_3	0.99	1.10	82, 78
17	A_1	B_1	$\nu_{21} + \nu_{26} - \nu_{26}$	914.539	914.475	(−)	0.064	0.91	[0.97]	0.93	0.99	1.06				0, −4
18	B_1	A_1	$\nu_{21} + 2\nu_{26} - 2\nu_{26}$	913.676	913.538	(−)	0.138	1.11	[0.97]	1.14	1.01	0.89				−4, −8
19	A_2	A_1	ν_{16}	859.77	858.127	(+)	1.643	0.67	[Δ_0]	0.69	0.98	1.42	p_2/p_1	0.75	1.09	8
20	B_2	B_1	$\nu_{16} + \nu_{26} - \nu_{26}$	860.55	858.56	(+)	1.99	1.02	[0.97]	1.04	0.99	0.87				4, −4
21	A_1	A_2	$\nu_{16} + \nu_{19} - \nu_{19}$	857.58	856.34	(+)	1.24	0.63	[0.61]	1.03	0.98	0.95	p_2/p_2	0.98	0.95	47, 39
22	A_1	A_1	ν_{10}	950.84	950.84	(−)	0.00	0. 97	[Δ_0]	1.00	1.00	1.00				2
23	A_2	A_2	$\nu_{10} + \nu_{19} - \nu_{19}$	951.36	951.19	(−)	0.17	0. 78	[0.61]	1.28	1.00	0.78	p_2/p_2	1.00	0.78	41, 39
24	A_1	A_1	ν_{11}	873.92	873.89	(−)	0.03	1. 00	[Δ_0]	1.03	1.01	0.98				−3
25	A_2	A_2	$\nu_{11} + \nu_{19} - \nu_{19}$	874.12	874.04	(−)	0.08	0.69	[0.61]	1.13	1.01	0.89	p_2/p_2	1.01	0.89	36, 39
26	B_1	A_1	ν_{23}	715.72	715.72	(−)	0.00	0.97	[Δ_0]	1.00	1.00	1.00				0
27	A_1	B_1	$\nu_{23} + \nu_{26} - \nu_{26}$	715.88	715.88	(−)	0.00	0.97	[0.97]	1.00	1.00	1.00				−4, −4
28	B_1	A_1	$\nu_{23} + 2\nu_{26} - 2\nu_{26}$	716.37	716.37	(−)	0.00	0.97	[0.97]	1.00	1.00	1.00				−8, −8
29	A_1	B_1	$\nu_{23} + 3\nu_{26} - 3\nu_{26}$	716.90	716.89	(−)	0.01	0.98	[0.97]	1.01	1.00	0.99				−12, −12
30	B_1	A_1	$\nu_{23} + 4\nu_{26} - 4\nu_{26}$	717.80	717.77	(−)	0.03	1.00	[0.97]	1.03	1.00	0.97				−16, −16
31	B_2	A_2	$\nu_{23} + \nu_{19} - \nu_{19}$	715.37	715.28	(−)	0.09	0.70	[0.61]	1.15	1.00	0.87	p_2/p_2	1.00	0.87	38, 39

[a–e] As in Table 1.

TABLE 5: ν_{37b} (high frequency) Tunneling Doublet and Hot Band Transitions

	transition[a]			doublet origin		doublet separation	state splittings[b]	
τ	U	L	assignment	ν^{hi}	ν^{lo}	$\lvert\Delta' \pm \Delta''\rvert$	Δ'[c]	Δ''
32	A_1	A_1	ν_{37b}	754.525	753.724	0.80	none	[$\sim\Delta_0$]
33	B_1	A_2	$\nu_{37b} + \nu_{19} - \nu_{19}$	752.15	751.45	0.70	none	[$\sim$0.6]
34	A_1	A_1	$\nu_{37b} + 2\nu_{19} - 2\nu_{19}$	750.10	749.57	0.53	none	[$\sim$0.4]

[a] See Table 3. See Figures 10A and 15. [b] See Table 3. [c] See Figure 15 and text.

process. The presence of these tautomerization path-passive states is not surprising; what is surprising is the many putatively inert vibrational states that participate strongly in the tautomerization process. Atom displacements occurring in the A_2 and B_2 vibrations of tropolone are inherently asymmetrical across the molecule and therefore inherently tautomerization path-active. Further, the vibrational displacements for some A_1 and B_1 fundamentals in the G_4 group are also sufficiently asymmetrical across the molecule to predict dynamical complexity and the quenching of tunneling through an increase of the tunneling path length when they are excited.

5. IR Observations on Tautomerization Path-active Quasiharmonic Vibrations

***ν_{22}* COH Torsion and *ν_{19}* OCCO/Skeletal Twisting Transitions.** A progression of Q branch absorptions extending from 752 cm^{-1} toward longer wavelengths is clearly shown in Figure 9A. The spectral doublets near 752 and 754 cm^{-1} are identified as cold bands by a sharp peak at 752 with a shoulder at 754 cm^{-1} in the IR spectrum of Ne-isolated Tp-oh.[24] A peak at 743 cm^{-1} in that spectrum is not matched by a nearby sharp type A Q branch in the vapor phase spectrum near the 743 cm^{-1}

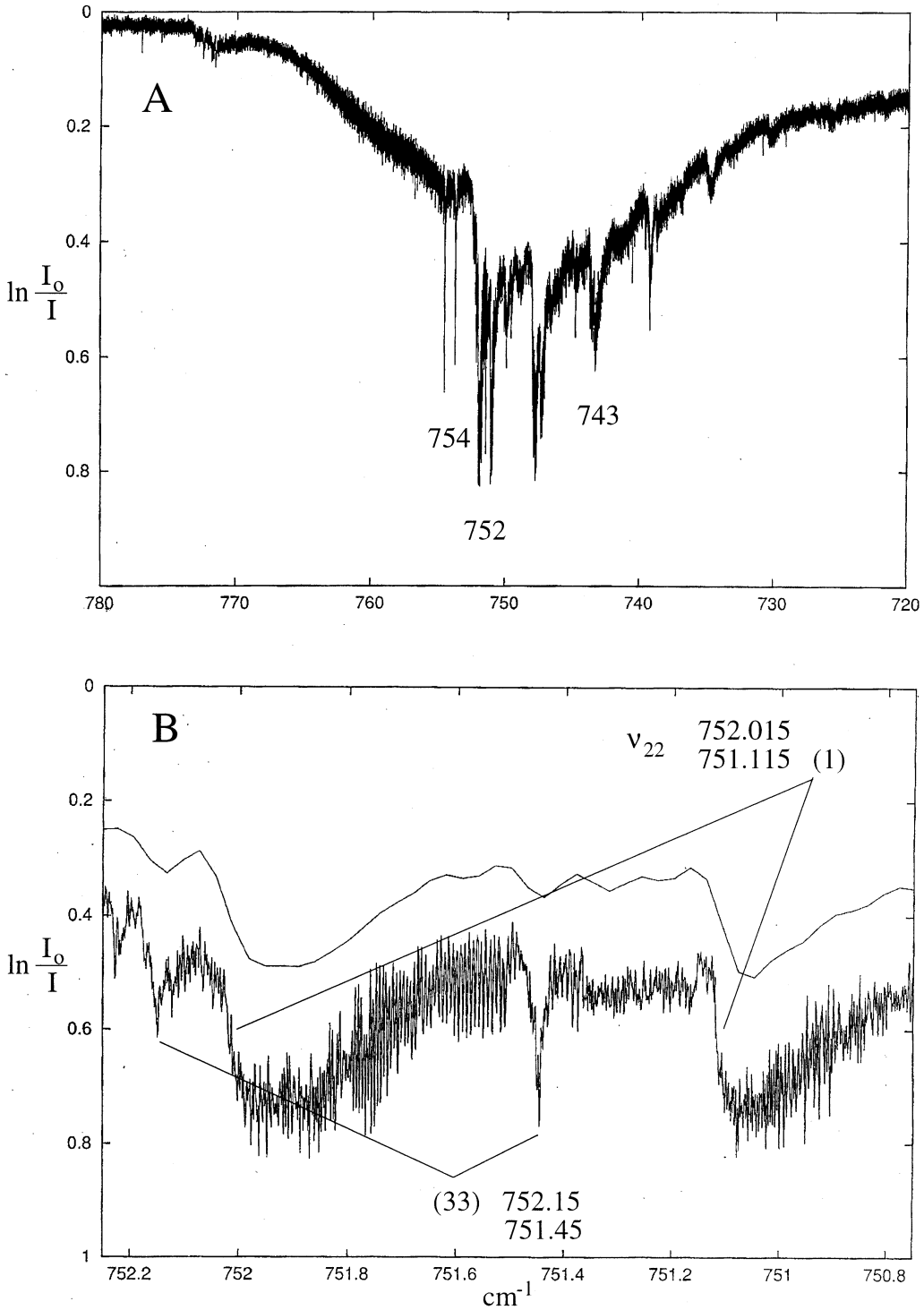

Figure 9. (A) Survey spectrum of the ν_{22} COH torsional region around 752 cm^{-1}. (B) Closeup of the ν_{22} spectral doublet region under resolutions of 0.1 and 0.0025 cm^{-1}. Identifications τ are parenthesized (cf. Tables 3−5).

member of the 752 cm^{-1} progression. The 754 and 743 cm^{-1} cold band transitions in Ne/Tp-oh were attributed[24,25] to tunneling structure of the nascent tautomerization vibration ν_{37}, and they are discussed in section 7.

The intense 752 cm^{-1} absorption is due to ν_{22}, the COH torsion fundamental, and the Q_{22} normal coordinate is shown in Figures 3 and 7A. The structure in Figure 9A appears as band scalloping at 752 and at 555 cm^{-1} in lower resolution spectra[24] of vapor phase Tp-oh and Tp-od, respectively. A 1.50 cm^{-1} segment of the spectrum spanning the 752 cm^{-1} doublet at 0.1 and 0.0025 cm^{-1} resolutions is shown in Figure 9B. Each Q branch region for ν_{22} is spread over a width of about 0.3 cm^{-1} to suggest appreciable differences between the upper state and lower state vibration-contortion-rotation parameters. As illustrated, the high-frequency edges of the contours are used to estimate band origins for the 752 cm^{-1} doublet and its hot band progression. The values 752.015 and 751.115 cm^{-1} for ν_{22} yield the spectral doublet separation $|\Delta_{22} - \Delta_0| = 0.900$ cm^{-1}, and $\Delta_0 = 0.974$ cm^{-1} then fixes Δ_{22} at either 0.074 or 1.874 cm^{-1}. The former value is chosen with support from the

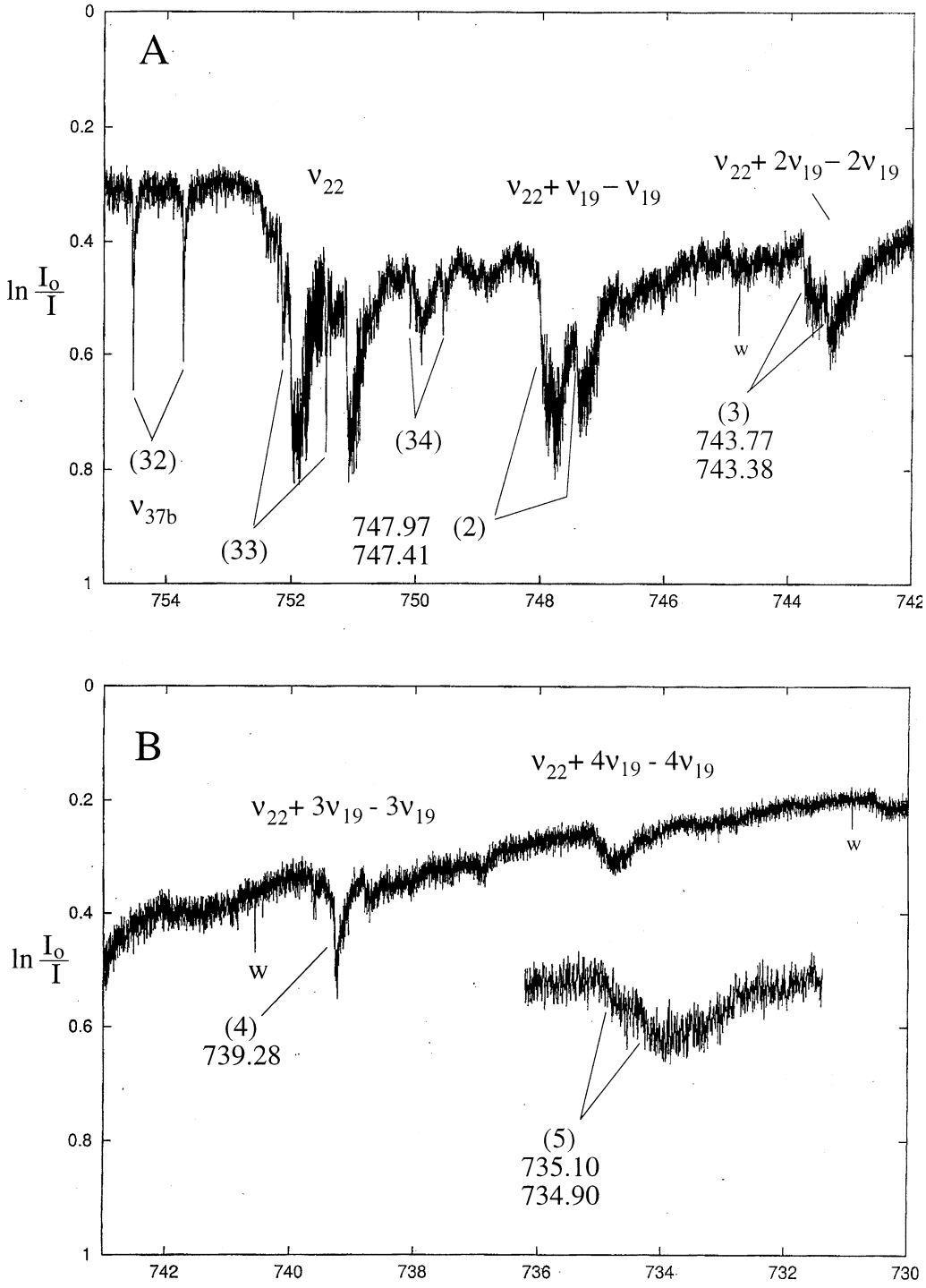

Figure 10. View of the 730−755 cm^{-1} spectral region showing $\nu_{22} + N_{19}\nu_{19}$ hot band progression. Transitions due to water vapor are labeled "w".

$\Delta E_B(\omega_{22},\tau = 1) = 366\ cm^{-1}$ barrier adjustment listed in Table 3. The ratio $f^{obs}_{\tau=1} = \Delta_{22}/\Delta_0 = 0.076$ indicates the tunneling is quenched relative to Δ_0 by more than an order of magnitude in the fundamental COH torsional state. The ratio $f^{cal}_{\tau=1} = 0.43$ computed using paths p_1/p_1 is lowered to 0.101 upon using paths p_5/p_1 as seen in Table 3. The R^{cal}_{obs} ratio for the ν_{22} fundamental is therefore decreased from ~6 to ~1 by a 12% increase of the effective tunneling path length in the ν_{22} state (half-distance: 0.287 Å increased to 0.321 Å). The modified R^{cal}_{obs} value is marked by the small white circle at $\tau = 1$ in Figure 8.

Upper state and lower state tunneling splittings of the hot band progression $\nu_{22} + N_{19}\nu_{19} - N_{19}\nu_{19}$, with $N_{19} = N = 1, 2, \cdots$, are symbolized as $\Delta' = \Delta^{1\ N}_{22\ 19}$ and $\Delta'' = \Delta^{0\ N}_{22\ 19} = \Delta^{N}_{19}$, respectively. Then $|\Delta^{1\ N}_{22\ 19} - \Delta^{0\ N}_{22\ 19}|$ is the spectral doublet separation. Known values for the small upper state splittings would allow the lower state splittings Δ^{N}_{19}, i.e., tunneling splittings for the ν_{19} IR fundamental and its overtones, to be obtained from the observed doublet separations. With this goal the upper state splittings $\Delta^{1\ N}_{22\ 19}$ are taken as decreasing in direct proportion to the Δ^{N}_{19} values obtained for S_1 Tp-oh[4] by combining the laser-induced fluorescence spectrum with Δ_0. This yields the estimates $\Delta^{1\ N}_{22\ 19} = 0.074$, 0.047, 0.031, 0.025, and 0.021 for $N = N_{19} = 0$ to 4 as entered for Δ' in lines 1−5 of Table 3.

The hot band Q branches are shown more clearly in Figure 10. As N_{19} increases the higher frequency Q branch weakens

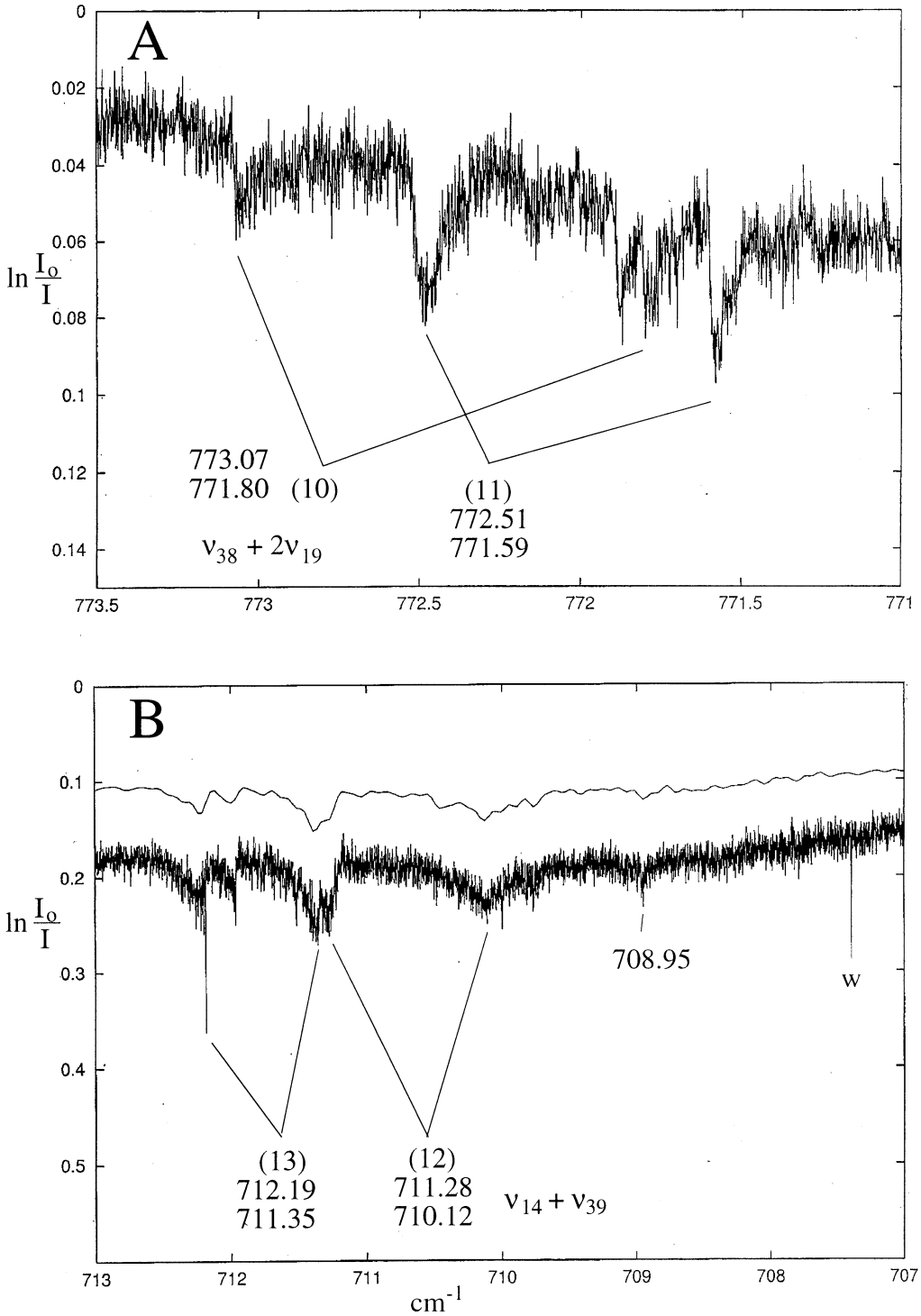

Figure 11. (A) The $\nu_{38} + 2\nu_{19}$ combination band transitions near 772 cm^{-1}. (B) The $\nu_{14} + \nu_{39}$ combination band transitions near 712 cm^{-1}.

relative to its partner, and only one Q branch origin can be reasonably estimated in the 739 cm^{-1} ($N_{19} = 3$) region. Appearances of the various vibration-contortion-rotation IR absorption profiles of tropolone are expected to vary considerably due to its double-minimum effective PES, and the behavior in Figure 10 anticipates extremely sharp Q branch profiles observed for several tautomerization path-passive quasiharmonic transitions. Combined with the $\Delta' = \Delta_{22\ 19}^{1\ N}$ upper states estimated above, the hot band spectral doublets produce $\Delta'' = \Delta_{22\ 19}^{0\ N} = \Delta_{19}^{N} = 0.61$, 0.42, and 0.22 cm^{-1} for the $N_{19} = 1$, 2, and 4 states as listed in lines 2−5 of Table 3. The large R_{obs}^{cal} values for paths p_1/p_1 (cf. Figures 7 and 8), show ν_{19} is a path-active vibration, and using paths 2−4 for the Δ_{19}^{N} states yields the near-unity R_{obs}^{cal} values listed in Table 3 and shown as white circles in Figure 8. The resulting p_2, p_3, and p_4 pathways are used as a base wherever the $N_{19}\nu_{19}$ states are encountered. Thus, paths p_6/p_2, p_7/p_3, p_7/p_4 and p_7/p_4 are systematically chosen as estimated extended paths of the Δ' and Δ'' states of the $\nu_{22} + N\nu_{19} - N\nu_{19}$ hot band progression as presented in lines 2−5 in Table 3 and in Figure 8.

As seen in Table 3 the $\Delta E_B(\tau)$ values involving ν_{19} are much smaller than those for ν_{22}. On the other hand, the asymmetrical vibrational displacements accompanying the tautomerization process for ν_{19} (cf. Figure 7A) inject dynamical complexity and

the consequential quenching of tunneling into the mechanism. The decreasing $\Delta^{0\ N}_{22\ 19} = \Delta^{N}_{19}$ splitting values for S_0 tropolone parallel behavior for the much larger splittings observed for S_1 tropolone.[4] The lowest frequency fundamentals in S_1 and S_0 tropolone are $\nu_{26} = 38$ and $\nu_{19} = 110$ cm^{-1}, respectively.

***ν*$_{38}$ + 2*ν*$_{19}$ Combination State.** A weak IR absorption at 774 cm^{-1} and a strong absorption at 771.3 cm^{-1} are found in the spectra of Ne/Tp-oh and Ne/Tp-od, respectively,[24] and the weak absorption of gaseous Tp-oh near 773 cm^{-1} is shown in Figures 9A and 11A. The isotopomer transitions were important to identifying the tunneling structure[24,25] for ν_{37}, and their intensity behaviors (including solvation effects) have inherent interest. They were previously assigned[24] as $\nu_{13} + \nu_{39}$ coupled in anharmonic resonance networks to other binary combination states, however, the resulting anharmonic frequency shifts are large relative to similar assignments in the spectra. They are reassigned here as $\nu_{38} + 2\nu_{19,}$ i.e., as 552 + 2(110) = 772 vs 774 cm^{-1} observed for Tp-oh and 550 + 2(109) = 768 vs 771.3 cm^{-1} observed for Tp-od, with support for the B_2 ternary combination states provided by type A Q branch spikes separated by $\Delta' + \Delta''$ (cf. Figure 5 for the Z transition dipole). The peaks at 773.07 and 771.80 cm^{-1} yield the spectral doublet separation 1.27 cm^{-1} and, with $\Delta'' = \Delta_0$, $\Delta' = \Delta^{1\ 2}_{38\ 19} = 0.30$ cm^{-1} as entered in line 10 of Table 3. The value $R^{cal}_{obs} = 2.70$ calculated for model paths p_1/p_1 falls to 1.45 on using paths p_3/p_1 as shown in Table 3 and Figure 8.

Figures 3 and 4 show the MP2/GEN-computed IR absorbances for ν_{38} and ν_{19} are very weak, but that the C(4), C(6), and C(7) atoms are prominent in both normal coordinates to suggest conditions favorable for the effective anharmonic coupling of ν_{38} and ν_{19}. The $\nu_{38} + 2\nu_{19}$ and $\nu_{38} + 3\nu_{19}$ combination states are believed to enter into similar anharmonic resonance networks, and the comparatively intense transitions in Figure 11A are assigned as the $(\nu_{38} + 2\nu_{19}) + \nu_{19} - \nu_{19}$ hot band doublet (line 11 of Table 3). The hot bands appear to be slightly more intense than the cold bands despite their Boltzmann factors. This anharmonic phenomenon is consistent with the above-noted sensitivity of the IR absorbance involving these vibrational states to the effects of CCl_4 solvation and to OH···O deuteration.

***ν*$_{14}$ + *ν*$_{39}$ Combination State.** Ne/Tp-oh samples have a weak IR transition at 711.5 cm^{-1}, and Figure 11B shows Q branches of the doubled $\nu_{14} + \nu_{39}$ cold band and $\nu_{14} + \nu_{39} + \nu_{19} - \nu_{19}$ hot band transitions of Tp-oh vapor. The appearance and assignments of the spectra in Figure 11A (lines 10 and 11 of Table 3) and Figure 11B (lines 12 and 13) are similar, with the relatively strong quenching of tunneling present in both cases.

IR transitions for the ν_{13}, ν_{14}, and ν_{39} fundamentals have been observed (Table 1), and the MP2/GEN Q_{13}, Q_{14}, and Q_{39} normal coordinates appear in Figure 4, but tunneling splittings for these fundamentals have not yet been resolved. The $\nu_{14} + \nu_{39}$ analysis is of interest with respect to the $\Delta E_B(\omega_{14})$, $\Delta E_B(\omega_{13})$, Δ_{13},and Δ_{14} values. It is difficult to unambiguously correlate the MP2/GEN-computed A_1 vibrational states of the C_{2v} SP configuration at 411 and 719 cm^{-1} with the computed ω_{13} and ω_{14} fundamentals of the tautomer. The correlation shown in Figure 4 produces $\Delta E_B(\omega_{13}) = -30$ and $\Delta E_B(\omega_{14}) = 355$ cm^{-1}, with $\Delta E_B(\omega_{13}) = 719-441 = 278$ cm^{-1} and $\Delta E_B(\omega_{14}) = 411-364 = 47$ cm^{-1} produced by the alternative. The large $\Delta E_B(\omega_{14})$ value is favored by the analysis in Table 3, which leaves $\Delta E_B(\omega_{13}) = -30$ cm^{-1} and the suggestion $\Delta_{13} > \Delta_0$ for the ν_{13} fundamental at 436 cm^{-1}. Figure 4 shows Q_{13} is the nominal O···O stretching fundamental (with in-phase HC(7)···C(3)H cross-ring stretching also involved). The Q_{13} coordinate intuitively suggests tunneling enhancement in the ν_{13} excited state, as reinforced by the negative $\Delta E_B(\omega_{13})$ value, although the small asymmetries present in Q_{13} suggest a modest quenching contribution may oppose the projected enhancement. Single level laser fluorescence studies by Sekiya, Nagashima, and Nishimura[6] and by Alves et al.,[40] lack the spectral resolution to reliably examine tunneling splittings for ν_{13} and ν_{14} in the S_0 state, but in the S_1 electronic state ν_{14} (nominal O···O stretching) and ν_{13} are assigned as similarly split doublets:[6] $\nu_{14} = 296$, 326 cm^{-1} and $\nu_{13} = 414$, 446 cm^{-1}. The 30 and 32 cm^{-1} tunneling splittings in S_1 Tp-oh are to be compared with $\Delta_0 = 19$ cm^{-1} in the S_1 state. In S_0 Tp-oh Δ_{14} is small, with only ν_{13} predicted to show tunneling enhancement. The ν_{13} fundamentals of S_0 and S_1 Tp-oh have similar frequencies; perhaps in S_0 Tp-oh it will be found that Δ_{13} is about 1.6 cm^{-1}, i.e., $\sim 1.6 = 32(0.97/19)$ cm^{-1}.

6. IR Observations on Tautomerization-Path-Passive Quasiharmonic Vibrations

***ν*$_{21}$ and *ν*$_{16}$ CH Wagging States.** In Figure 12A, the remarkable Q branch structures observed using 0.0025 cm^{-1} resolution on the central Q branch region of ν_{21} around 915 cm^{-1} are shown. The sharp peaks suggest the upper state and lower state vibration-contortion-rotation parameters are very similar. $\Delta E_B(\omega_{21},\tau = 14)$ is only 4 cm^{-1}, cf. Table 4, and Q_{21}, a B_1 mode (Figure 3), is quite symmetrical across the molecule, although there is a small COH torsional component. These results suggest Δ_{21} should be moderately less than Δ_0.

The two most intense peaks in Figure 12A are assigned as the type C Q branches of the ν_{21} cold band doublet (the Ne/Tp-oh transition is at 916.6 cm^{-1}) and the remaining peaks are assigned as the Q branch doublets of hot bands. Figure 12B shows the $\sim$0.01 cm^{-1} widths of the ν_{21} doublet peaks at 0.0025 cm^{-1} resolution, their smoothness, and their relative inconspicuousness at 0.1 cm^{-1} resolution. The doublet separation $|\Delta^{1\ 0}_{22\ 19} - \Delta_0| = 0.200$ cm^{-1} yields the candidates 0.774 and 1.174 cm^{-1} for $\Delta^{1\ 0}_{22\ 19}$. The 0.774 cm^{-1} value, i.e., $\Delta_{21} = 0.79\Delta_0$, verifies the moderate expected quenching of tunneling noted above. Doublets assigned to the $\nu_{21} + \nu_{19} - \nu_{19}$ and $\nu_{21} + 2\nu_{19} - 2\nu_{19}$ hot bands have coincidentally the same separation, 0.042 cm^{-1}, cf. Figure 12A and lines 15, 16 of Table 4. The previously determined $\Delta^{0\ 1}_{22\ 19} = 0.61$, and $\Delta^{0\ 2}_{21\ 19} = 0.42$ cm^{-1} values (Table 3) for the lower states yield similar values for the upper state splittings, 0.65 and 0.38 cm^{-1}, as expected. The two remaining hot band doublets in Figure 12A are tentatively assigned as $\nu_{21} + N_{26}\nu_{26} - N_{26}\nu_{26}$ in lines 17, 18 of Table 4. The $\Delta E_B(\omega_{26})$ value is -4 cm^{-1} (Table 2) and the form of Q_{26} suggests an opposing slight quenching of tunneling. Lacking experimental evidence, the value $\Delta^{N}_{26} = \Delta_0 = 0.97$ cm^{-1} is used for $N_{26}\nu_{26}$ wherever these states arise. Table 4 and Figure 8 show R^{cal}_{obs} values for $\tau = 17$ and 18 are near unity for the model paths p_1/p_1 as well as for the extended paths required by the $N_{19}\nu_{19}$ hot bands.

The species A_2 ν_{16} fundamental has type C rotational contours and the $\Delta' + \Delta''$ spectral doublet separation. Q_{16} has asymmetrical CH wagging displacements accompanied by a small COH torsion displacement as shown in Figure 3, and the $\Delta E_B(\omega_{16}, \tau = 19)$ value is 8 cm^{-1}. The data and analysis are shown in Figure 13A and collected in lines 19−21 of Table 4 and in Figure 8. The 858.127 transition is strongly spiked while the other Q branch absorptions are more spread out and structured. The Ne/Tp-oh transition is at 860.1 cm^{-1}.

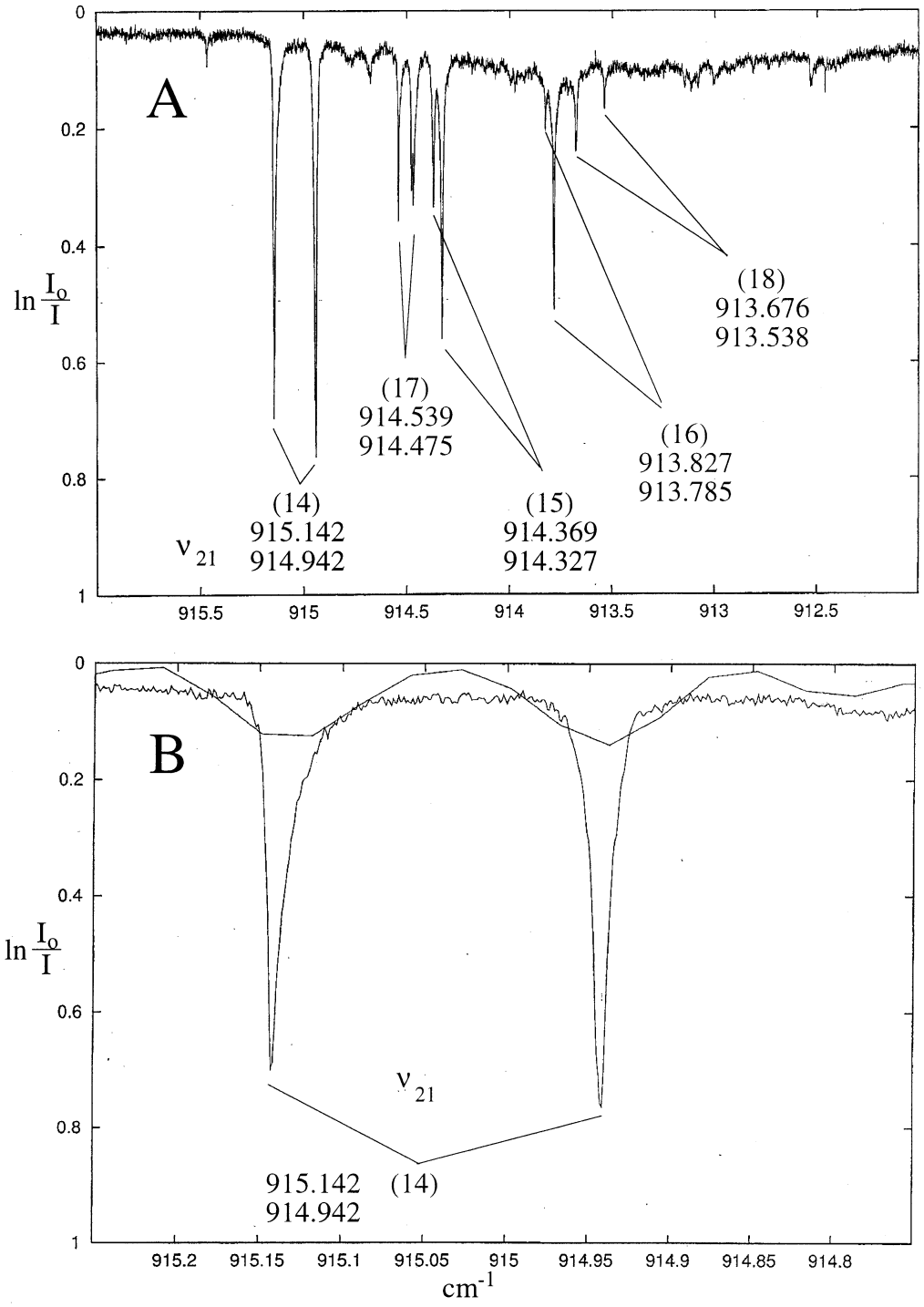

Figure 12. (A) Central Q branch region of the ν_{21} CH wagging transition near 915 cm^{-1}. (B) The ν_{21} spectral doublet at resolutions of 0.1 and 0.0025 cm^{-1}.

***ν*$_{10}$ and *ν*$_{11}$ CH Rocking/Skeletal Deformation States.** The central Q branch region of ν_{10} near 951 cm^{-1} is shown in Figure 13B, where the 950.84 cm^{-1} spike is assigned as the unresolved cold band doublet (the Ne/Tp-oh transition is 951.9 cm^{-1}), and Q branches at 951.36 and 951.19 cm^{-1} are assigned as a blue shifted $\nu_{10} + \nu_{19} - \nu_{19}$ hot band. Figure 4 shows that Q_{10}, species A_1, is dominated by symmetrical in-plane CCH rocking phased to suggest a dominant type A rotational contour with minimal input of transition dipole on the Y axis. The transitions are summarized in lines 22, 23 of Table 4 and in Figure 8. The central Q branch region of ν_{11} near 874 cm^{-1} is shown in Figure 13C, with Q_{11} shown in Figure 4. Q_{11}, species A_1, has symmetrical CCH rocking and CCC angle bending displacements leading, like ν_{10}, to a dominant type A rotational profile. The analysis closely parallels that for ν_{10} as seen in Figure 13C, lines 24, 25 of Table 4, and Figure 8. The Ne/Tp-oh transition is 875.4 cm^{-1}.

***ν*$_{23}$ Symmetrical CH Wagging State.** The ν_{23} fundamental, 714.8 cm^{-1} in Ne/Tp-oh, is the symmetric CH wagging mode as seen in Figure 3 for Q_{23}, with a small amount of ring-deformation. With $\Delta E_B(\omega_{23},\tau = 26) = 0$ and a virtually nil OH$\cdot\cdot\cdot$O contribution to Q_{23}, the effect of ν_{23} on the tautomerization is expected to be minimal, with sharp Q branch structures resembling those for ν_{21} (cf. Figure 12) reasonably expected. Figure 14 shows many sharp peaks occur in the central Q branch region of ν_{23}, and that they are spread into interesting patterns

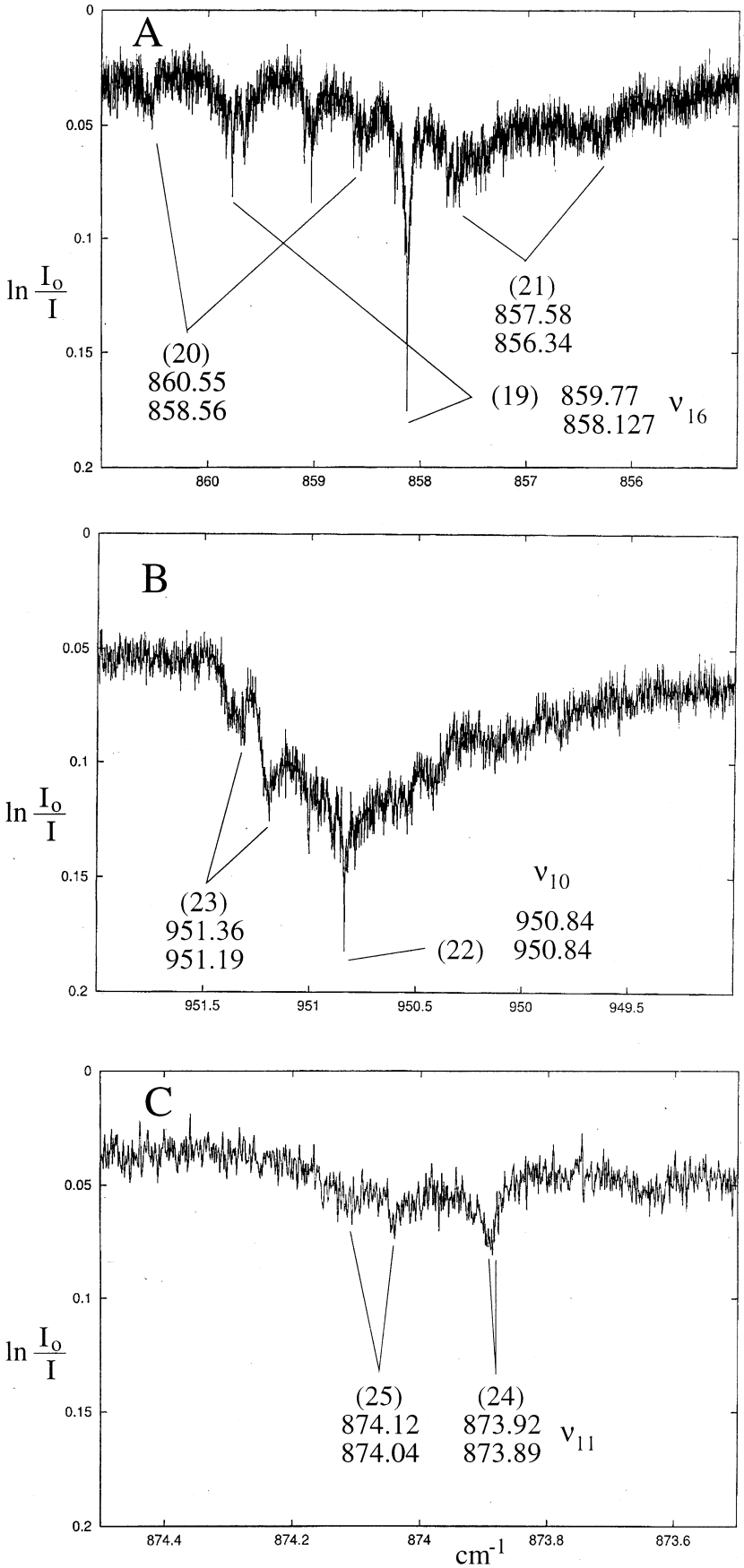

Figure 13. (A) Central Q branch region of the ν_{16} asymmetrical CH wag/COH torsion vibration near 858 cm^{-1}. (B) Central Q branch region of the ν_{10} symmetrical CCH rock/ring deformation vibration near 951 cm^{-1}. (C) Central Q branch region of the ν_{11} transition near 874 cm^{-1}.

for the higher ν_{26} hot band excitations. The present tentative introductory analysis of the data in lines 26−31 in Table 4 proposes an unresolved cold band spectral doublet at 715.72 cm^{-1} (the Ne/Tp-oh transition is at 714.8 cm^{-1}) with the blue-

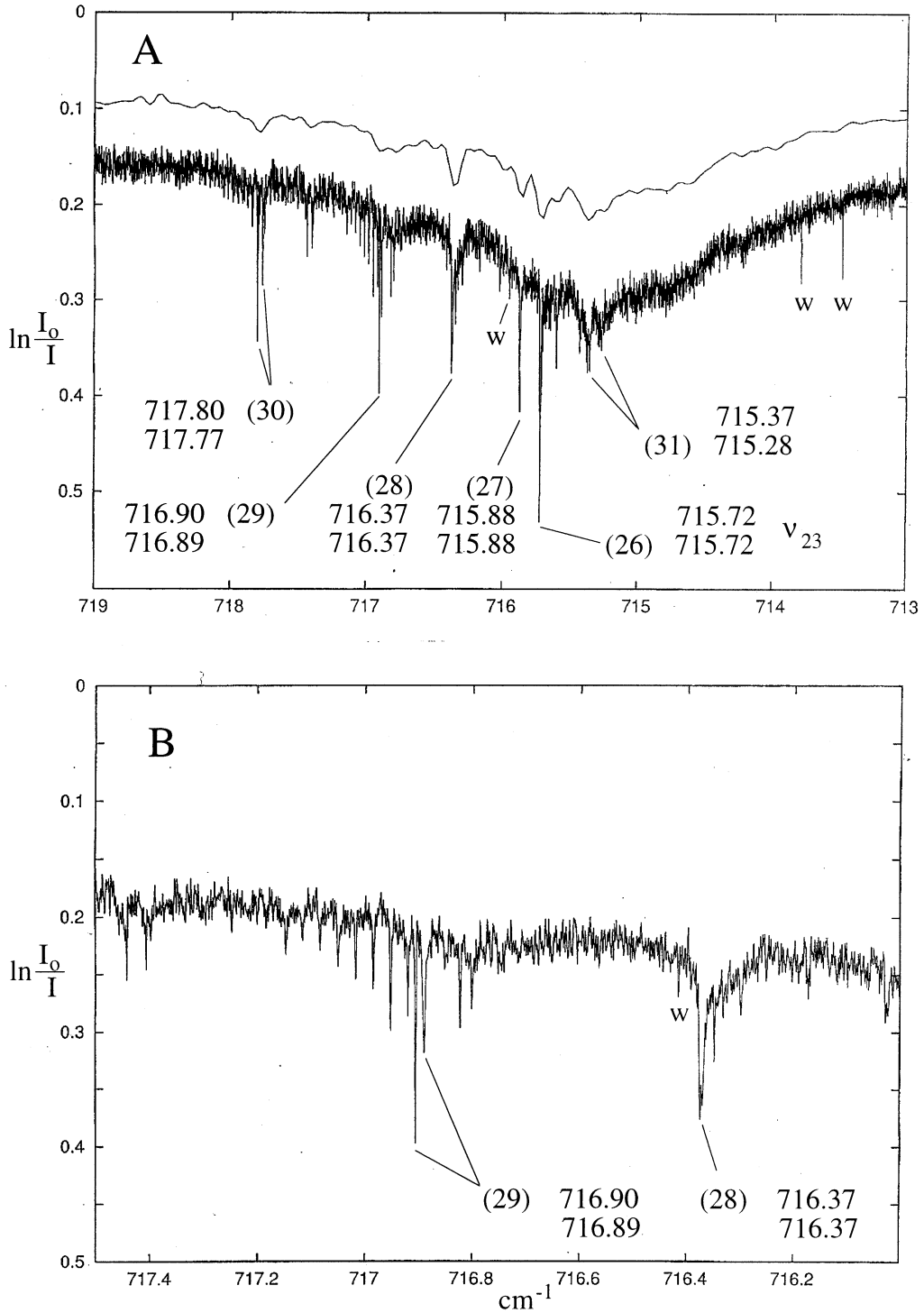

Figure 14. (A) Central Q branch region of the ν_{23} symmetrical CH wagging vibration near 715 cm^{-1}. (B) Closer view of vibration-contortion-rotation structure near 717 cm^{-1}.

shifted hot band progression $\nu_{23} + N_{26}\nu_{26} - N_{26}\nu_{26}$ ($N_{26} = 1-4$) also showing very small doublet separations. Hot bands in ν_{19} occur throughout the tropolone IR absorption spectrum and in this region the $\nu_{23} + \nu_{19} - \nu_{19}$ transition is discernible as listed in line 31 of Table 4. Like many of the tropolone fundamentals, ν_{23} is believed to participate in an anharmonic resonance network and it is possible that these interactions contribute to the complex spectral pattern resolved in Figure 14. There is a weak Ne/Tp-oh transition at 720.3 cm^{-1}, but no evidence for a sharp Q branch is observed in the high-resolution spectrum around 720 cm^{-1}.

7. FTIR Observations Concerning the ν_{37} Tautomerization Transition

Figures 4 and 2 suggest the ν_{37} contortion (nascent tautomerization) vibration generates transition dipoles on the Y and Z inertial principal axes to predict a quartet of tunneling transitions with origins separated by $|\Delta_{37} \pm \Delta_0|$ as shown on the right side of Figure 15B. In the G_4 molecular symmetry group,[35] the ladder of ν_{37} contortional states with even valued and with odd valued contortional quantum numbers N_{con} have A_1 and B_2 irreducible representations, respectively. Δ_0 is given by the

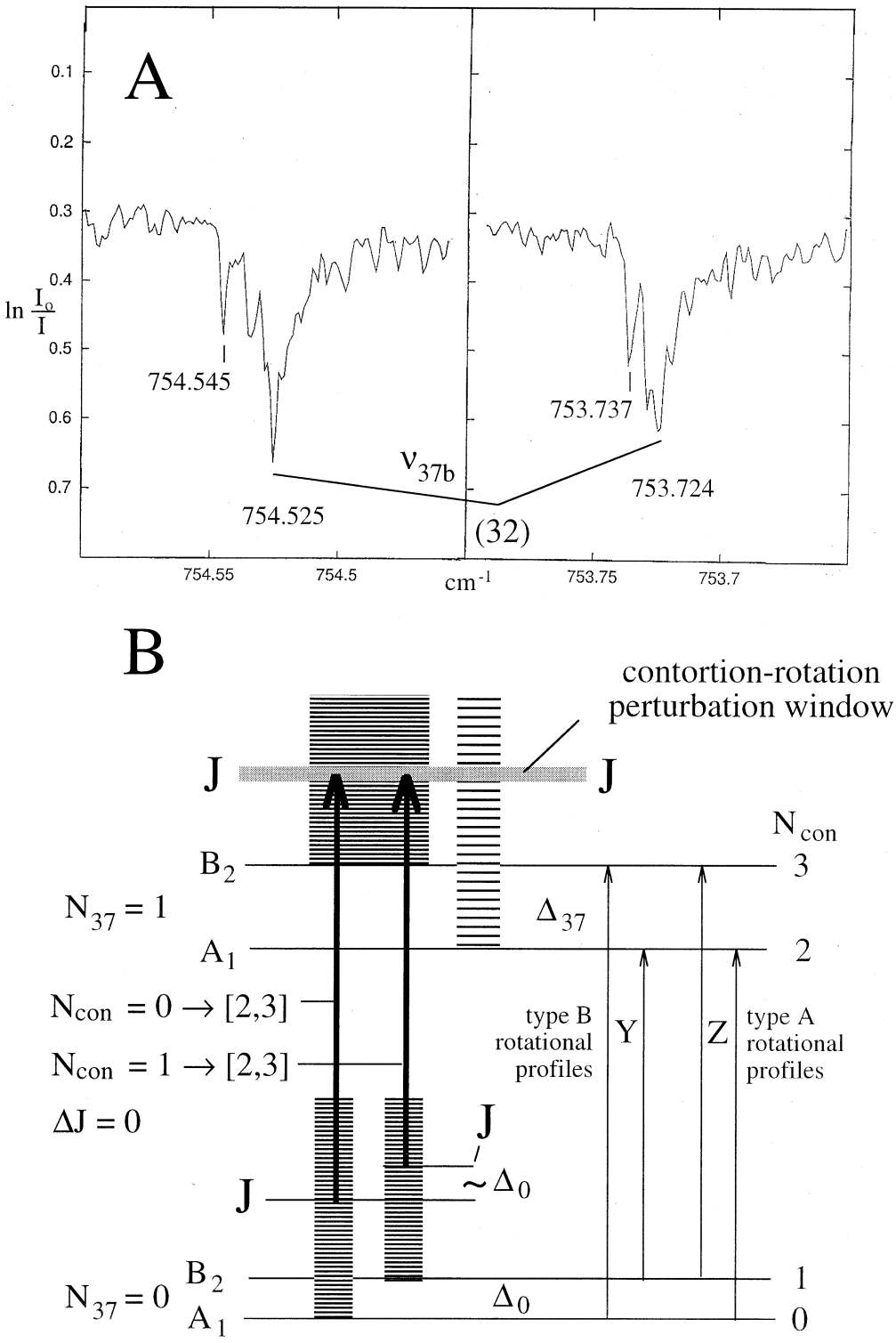

Figure 15. (A) Sharp upper state ν_{37} doublet components near 754 cm^{-1}. (B) Plausible origin of the 754 cm^{-1} doublet behavior as $\Delta J = 0$ transitions from the ZP states to a set of perturbationally mixed upper states. See text.

separation of the lowest B_2 and A_1 contortional states E($N_{37} = 0$, $N_{con} = 1$) and E($N_{37} = 0$, $N_{con} = 0$). The two type B transitions (Y transition dipole) are expected to be more intense than the two type A transitions (Z transition dipole).

IR transitions in Ne/Tp-oh at 743.4 and 754 cm^{-1} were assigned[24,25] as the ν_{37} tunneling doublet to establish the approximate $\Delta_0 + \Delta_{37}$ separation. In the vapor phase spectra the type B contours are lost in the background and their origins cannot be refined in the present work. As there is no evidence for sharp type A Q branch structure attributable to ν_{37} in the present gas-phase spectrum near 743 cm^{-1} it is clear the Z transition dipole is inherently weak. On the other hand, Figure 10A shows the 754 cm^{-1} cold band transition of Ne/Tp-oh appears as a doublet with very sharp Q branch apexes in the vapor phase spectrum. This doublet is not attributed to an overtone, combination, or spectral impurity state for arguments discussed previously.[24,25] The sharp absorptions are shown with the wavenumber scale expanded in Figure 15A. Each doublet component appears to be overlapped with background undulations, and to possess a rotational substructure of its own. The

spread of the Q branch absorption regions are each less than 0.05 cm^{-1}, and the estimated spectral doublet separation is 0.80 cm^{-1}, i.e., $0.82\Delta_0$.

Three points concerning the 754 cm^{-1} doublet warrant attention. First, the doublet separation is $0.82\Delta_0$. Second, the peak spreads are only ~0.05 cm^{-1} despite the high anharmonicity of the double-minimum PEF for ν_{37}. Third, there is no corresponding sharp Q branch structure for ν_{37} near 743 cm^{-1} (cf. Figure 10A). Each of these points is accommodated by behavior proposed in Figure 15B. This relies on the marked differences expected to occur between vibration-contortion-rotation parameter values in the ($N_{37} = 1$; $N_{con} = 2$) and ($N_{37} = 1$; $N_{con} = 3$) states. These are expected to differ from each other and from the ZP parameters.

Figure 15B suggests the differently spaced upper state contortion−rotation energy manifolds develop a narrow energy range wherein the *J* state manifolds become nearly degenerate. In this "perturbation window" the *J* states are strongly mixed through a vibration-contortion-rotation coupling that is not defined here. The observed doublet is then attributed to the pileup of $\Delta J = 0$ transitions from the lower states to these mixed upper states, i.e., to $N_{con} = 0 \rightarrow$ (mixed 2, 3) and $N_{con} = 1 \rightarrow$ (mixed 2, 3) transitions made equally allowed through the coupling perturbation. The quantification of this scenario provides an experimental−theoretical research challenge beyond the scope of the present article.

The 754 cm^{-1} doublet appears to be accompanied by ν_{19} hot band doublets at 752.15, 751.45 cm^{-1}, and at 750.10, 749.57 cm^{-1} as listed with the results for ν_{37b} in lines 32−34 of Table 5. These sharp peaks, reminiscent of the 754 cm^{-1} doublet peaks, are seen in Figures 8A and 9A.

8. Concluding Remarks

1. The first FTIR spectrum of gaseous tropolone at 0.0025 cm^{-1} spectral resolution cannot be rotationally resolved, but it clearly shows many Q branch spikes ranging from ~0.01 to 0.3 cm^{-1} in width that are associated with types A and C rotational contours. The Q branch peaks provide estimates for the tunneling doublet separations of 29 cold band and hot band quasiharmonic transitions of S_0 tropolone-oh in the 700 to 960 cm^{-1} region. The estimated spectral doublet separations relate to the upper state and lower state tunneling splittings through $|\Delta' \pm \Delta''|$, and lead to estimates for 26 tunneling splitting values ranging from near zero to 1.11 cm^{-1}. The $|\Delta' - \Delta''|$ versus $\Delta' + \Delta''$ doublet separations provide important confirmations of the irreducible representations for many vibrational states.

2. Some of the Q branch peaks for the quasiharmonic vibrations are very narrow with full-widths-at-half-maxima of ~0.01 cm^{-1}. These peaks occur for quasiharmonic vibrations showing virtually no interaction with the tautomerization process. Because each of the observed Q branch structures, whether narrow or broad, is composed of many $\Delta J = 0$ transitions the various observed unresolved shapes, resolved substructures, and very sharp spikes all invite attempts at more extensive analysis incorporating the molecular dynamics of the nonrigid tropolone molecule.

3. In this work, about half of the observed quasiharmonic vibrations that were examined have little influence on the tunneling, showing splittings $\Delta_V \approx \Delta_0$. For each fundamental of this type the normal modes and vibrational frequencies of the tautomer and C_{2v} saddlepoint geometries are very similar. For fundamentals which quench tunneling ($\Delta_V < \Delta_0$) the decreased tunneling splitting Δ_V derives from an increase in the tunneling barrier because [$\omega_V(C_{2v}$ SP) > ω_V (taut)] and/or and from an increase in the effective tunneling path length. The latter is heuristically attributed to dynamic complexity arising because the tautomerization must exchange quasiharmonic vibrational displacements between pairs of atoms that are located oppositely across the molecule from each other. The B_2 and A_2 fundamentals (G_4 molecular symmetry group) inherently require such an exchange of vibrational displacements but it also may occur, sometimes importantly, for vibrations with A_1 or B_1 symmetries. The spectra demonstrate that effects are exerted on the tunneling by excited vibrational states that might naively be expected to be inert, e.g., because of remoteness from the OHO grouping.

4. The {tunneling skeleton}{tunneling H atom} model previously applied to the vibrational and tautomerization properties of tropolone[24,25] is also strongly supported by the present results. Through MO-computed harmonic vibrational frequencies the model predicts vibrational state-specific barrier maxima for any excitation, and allows heuristic assessment of the effective tunneling path lengths for the path-active vibrations by providing predicted path-dependent tunneling splittings as well. In the present state of its development, the computed *ratios* of tunneling splittings were compared with the corresponding experimental values, and found to be in excellent agreement. The model's predictions showed the need for the reassignment of a combination transition to ($\nu_{38} + 2\nu_{19}$), and routinely handled the vibrationally induced enhancement of tunneling insofar as this topic arose in the present data set.

5. The FTIR observation of the gas phase doublet at 754 cm^{-1} supports the previous assignment[24,25] of the Ne/Tp-oh transitions at 754, 743.4 cm^{-1} (Ne/Tp-od transitions at 751.3, 741.4 cm^{-1}) to the tunneling doubled nascent tautomerization vibration ν_{37}. In the gas-phase, each of the Ne/Tp transitions should appear as a spectral doublet with the separation Δ_0 reflecting transitions with oscillating dipoles along the Z (weak IR) and Y (strong IR) principal inertial axes. The Z transition dipole is experimentally seen to be weak since type A Q branches are not observed near 743 cm^{-1}; however, there is a sharp spectral doublet with near-equal intensities at 754 cm^{-1}. This observation is rationalized by invoking a perturbation that strongly mixes the $\nu_{37}(N_{37} = 1, N_{con} = 2, J)$ and $\nu_{37}(N_{37} = 1, N_{con} = 3, J)$ states over a narrow range of nearly degenerate *J* states. The window of coupled upper states is taken as providing roughly equivalent $\Delta J = 0$ transitions from the $N_{con} = 0$ and $N_{con} = 1$ lower states. The observed doublet separation of $0.82\Delta_0$ (rather than Δ_0) supports the argument that the perturbation acts over a narrow range of states with relatively high *J* values.

6. The past and present results that have been obtained for tropolone appear to probe, on a tractable level, the phenomena needed to develop practical understanding concerning the active site behavior in enzyme catalyzed H transfer reactions. The present work clearly demonstrates the skeletal vibrational complexity that can arise, and the need for multidimensional approaches to the tunneling coordinate in large molecules. It helps select the nature of "remote" modes, which may enter the tunneling phenomena in their excited states. The work re-emphasizes the important role of actual heavy atom tunneling in tropolone by a further observational refinement of its spectral tunneling structure. The final paragraph in the Introduction briefly discusses the potential applicability of tropolones as prototypes for characterizing phenomena that are likely to also occur in large systems such as H transfer enzymes.

7. The present FTIR spectra were recorded at 298 K. The hot band assignments correlate well with the quenching activity attributed to $N_{19}\nu_{19}$ states and with the passiveness attributed

to $N_{26}\nu_{26}$ states, and the Ne matrix-isolation IR data help support the cold band assignments. However, future high-resolution IR absorption spectra at additional temperatures are warranted—not only to confirm and/or reassess hot band behaviors, but also to provide a solid base of quantitative absorbance/frequency data that can be applied as additional handles to the state-dependent resonance and intramolecular tunneling interactions.

Acknowledgment. R.L.R. is grateful to the Robert A. Welch Foundation for long-time support of research on the behavior of hydrogen bonded molecules. A portion of the research described in this paper was performed at the W. R. Wiley Environmental Molecular Sciences Laboratory, a national scientific user facility sponsored by the Department of Energy's Office of Biological and Environmental Research and located at Pacific Northwest National Laboratory. Pacific Northwest National Laboratory is operated for the U. S. Department of Energy by Battelle under Contract DE-AC06-76RLO 1830. The authors are grateful to T. E. Redington for discussions of this work and for reading the manuscript.

References and Notes

(1) Alves, A. C. P.; Hollas, J. M. *Mol. Phys.* **1972**, *23*, 927.
(2) Alves, A. C. P.; Hollas, J. M. *Mol. Phys.* **1973**, *25*, 1305.
(3) Tomioka, Y.; Ito, M.; Mikami, N. *J. Phys. Chem.* **1983**, *87*, 4401.
(4) Redington, R. L.; Chen, Y.; Scherer, G. J.; Field, R. W. *J. Chem. Phys.* **1988**, *88*, 627.
(5) Redington. R. L.; Field, R. W. *Spectrochim. Acta A* **1989**, *45*, 41.
(6) Sekiya, H.; Nagashima, Y.; Nishimura, Y. *Bull. Chem. Soc. Jpn.* **1989**, *62*, 3229.
(7) Sekiya, H.; Nagashima, Y.; Nishimura, Y. *Chem. Phys. Lett.* **1989**, *160*, 581.
(8) Sekiya, H.; Nagashima, Y.; Nishimura, Y. *J. Chem. Phys.* **1990**, *92*, 5761.
(9) Sekiya, H.; Nagashima, Y.; Tsuji, T.; Nishimura, Y.; Mori, A.; Takeshita, H. *J. Phys. Chem.* **1991**, *95*, 10 311.
(10) Redington, R. L.; Redington, T. E.; Hunter, M. A.; Field, R. W. *J. Chem. Phys.* **1990**, *92*, 6456.
(11) Sekiya, H.; Sasaki, K.; Nishimura, Y.; Li, Z.-H.; Mori, A.; Takeshita, H. *Chem. Phys. Lett.* **1990**, *173*, 285.
(12) Sekiya, H.; Sasaki, K.; Nishimura, Y.; Mori, A.; Takeshita, H. *Chem. Phys. Lett.* **1990**, *174*, 133.
(13) Sekiya, H.; Takesue, H.; Nishimura, Y.; Li, Z.-H.; Mori, A.; Takeshita, H. *J. Chem. Phys.* **1990**, *92*, 2790.
(14) Sekiya, H.; Tsuji, T.; Ito, S.; Mori, A.; Takeshita, H.; Nishimura, Y. *J. Chem. Phys.* **1994**, *101*, 3465.
(15) Ensminger, F. A.; Plassard, J.; Zwier, R. S.; Hardinger, S. *J. Chem. Phys.* **1995**, *102*, 5246.
(16) Babamov, V. K. *Chem. Phys. Lett.* **1994**, *217*, 254.
(17) Vener, M. V.; Scheiner, S.; Sokolov, N. D. *J. Chem. Phys.* **1994**, *101*, 9755.
(18) Nash, J. J.; Zwier, T. S.; Jordan, K. D. *J. Chem. Phys.* **1995**, *102*, 5260.
(19) Takada, S.; Nakamura, H. *J. Chem. Phys.* **1995**, *103*, 353.
(20) Paz, J. J.; Moreno, M.; Lluch, J. M. *J. Chem. Phys.* **1995**, *103*, 353.
(21) Smedarchina, Z.; Siebrand, W.; Zgierski, M. Z. *J. Chem. Phys.* **1996**, *104*, 1203.
(22) Guo, Y.; Sewell, T. D.; Thompson, D. L. *J. Phys. Chem. A* **1998**, *102*, 5040.
(23) Wojcik, M. J. *J. Chem. Phys.* **2000**, *112*, 6322.
(24) Redington, R. L.; Redington, T. E.; Montgomery, J. M. *J. Chem. Phys.* **2000**, *113*, 2304.
(25) Redington, R. L. *J. Chem. Phys.* **2000**, *113*, 2319.
(26) Ikegami, Y. *Bull. Chem. Soc. Jpn.* **1961**, *34*, 94.
(27) Ikegami, Y. *Bull. Chem. Soc. Jpn.* **1963**, *36*, 1118.
(28) Frost, R. K.; Hagemeister, F. C.; Arrington, C. A.; Zwier T. S. *J. Chem. Phys.* **1996**, *105*, 2595.
(29) Tanaka, K.; Honjo, H.; Tanaka, T.; Kohguchi, H.; Ohshima, Y.; Endo, Y. *J. Chem. Phys.* **1999**, *110*, 1969.
(30) Kohen, A.; Klinman, J. P. *Chem. Biol.* **1999**, *6*, R191.
(31) Kohen, A.; Klinman, J. P. *Acc. Chem. Res.* **1998**, *31*, 398.
(32) Billeter, S. R.; Webb, S. P.; Iordanov, T.; Agarwal, P. K.; Hammes-Schiffer, S. *J. Chem. Phys.* **2001**, *114*, 6925.
(33) Antoniou, D.; Schwartz, S. D. *J. Phys. Chem.* **2001**, *105*, 5553.
(34) Ueda, T.; Shimanouchi, T. *J. Mol. Spectrosc.* **1968**, *28*, 350.
(35) Bunker, P. R.; Jensen, P. *Molecular Symmetry and Spectroscopy*, Second edition; NRC Research Press: Ottawa, 1998.
(36) Redington, R. L.; Bock, C. W. *J. Phys. Chem.* **1991**, *95*, 10 284.
(37) Frisch, M. J.; Trucks, G. W.; Schlegel, H. B.; Scuseria, G. E.; Robb, M. A.; Cheeseman, J. R.; Zakrzewski, V. G.; Montgomery, J. A., Jr.; Stratmann, R. E.; Burant, J. C.; Dapprich, S.; Millam, J. M.; Daniels, A. D.; Kudin, K. N.; Strain, M. C.; Farkas, O.; Tomasi, J.; Barone, V.; Cossi, M.; Cammi, R.; Mennucci, B.; Pomelli, C.; Adamo, C.; Clifford, S.; Ochterski, J.; Petersson, G. A.; Ayala, P. Y.; Cui, Q.; Morokuma, K.; Malick, D. K.; Rabuck, A. D.; Raghavachari, K.; Forseman, J. B.; Cioslowski, J.; Ortiz, J. V.; Stefanov, B. B.; Liu, B.; Liashenko, A.; Piskorz, P.; Komaromi, I.; Gomperts, R.; Martin, R. L.; Fox, D. J.; Keith. T.; Al-Laham, M. A.; Peng, C. Y.; Nanayakkara, A.; Gonzalez, C.; Challacombe, M.; Gill, P. M. W.; Johnson, B.; Chen. W.; Wong, M. W.; Andres, J. L.; Head-Gordon, M.; Replogle, E. S.; Pople, J. A. *Gaussian 98*, revision A.6; Gaussian, Inc.: Pittsburgh, PA, 1998.
(38) Permanent dipole moments were computed at the MP2/GEN[24,25] level. Dipole components expressed in the standard coordinate axes for the electrical charge distribution are $\mu_Y = 3.436$ and $\mu_Z = -2.833$ D. In this system, the center-of-mass is at Y, Z = −0.032, 0.031. The inertial axes are rotated 41.50 degrees CCW from the electrical axes.
(39) The lowest out-of-plane modes are 110, 177, and 271 cm^{-1} with Boltzmann factors 0.588 (0.639), 0.425 (0.486), and 0.270 (0.331) at 25 (80) °C, respectively. The lowest in-plane modes are 348, 364, and 441 cm^{-1} with Boltzmann factors 0.185 (0.241), 0.172 (0.226), and 0.119 (0.165).
(40) Alves, A. C. P.; Hollas, J. M.; Musa, H.; Ridley, T. *J. Mol. Spectrosc.* **1988**, *109*, 99.
(41) Jackman, L. M.; Trewella, J. C.; Haddon, R. C. *J. Am. Chem. Soc.* **1980**, *102*, 2519.
(42) A column added to Table 4 of ref 25 to include path E′ (p_5) would contain the values R(O···O) = 2.3113 Å; $\Delta S° = 0.3206$ Å; E[C_{2V} skel] = 1756 cm^{-1}; and $\beta = 37.969$. For $N_{27} = 0$ the value of α is 9.16 cm^{-1} and VS(eff, 37) [N_{27}], $\Delta S° = 0$ is 1765 cm^{-1}. $C_2 = -34\ 169$ and $C_4 = 166\ 215$.